Rate Dependence and Regulation of Action Potential and Calcium Transient in a Canine Cardiac Ventricular Cell Model

Thomas J. Hund, PhD; Yoram Rudy, PhD

Background—Computational biology is a powerful tool for elucidating arrhythmogenic mechanisms at the cellular level, where complex interactions between ionic processes determine behavior. A novel theoretical model of the canine ventricular epicardial action potential and calcium cycling was developed and used to investigate ionic mechanisms underlying Ca^{2+} transient (CaT) and action potential duration (APD) rate dependence.

Methods and Results—The Ca^{2+}/calmodulin-dependent protein kinase (CaMKII) regulatory pathway was integrated into the model, which included a novel Ca^{2+}-release formulation, Ca^{2+} subspace, dynamic chloride handling, and formulations for major ion currents based on canine ventricular data. Decreasing pacing cycle length from 8000 to 300 ms shortened APD primarily because of $I_{Ca(L)}$ reduction, with additional contributions from I_{to1}, I_{NaK}, and late I_{Na}. CaT amplitude increased as cycle length decreased from 8000 to 500 ms. This positive rate–dependent property depended on CaMKII activity.

Conclusions—CaMKII is an important determinant of the rate dependence of CaT but not of APD, which depends on ion-channel kinetics. The model of CaMKII regulation may serve as a paradigm for modeling effects of other regulatory pathways on cell function. **(*Circulation*. 2004;110:3168-3174.)**

Key Words: electrophysiology ■ action potentials ■ calcium ■ ion channels

The dependence of action potential duration (APD) and the Ca^{2+} transient (CaT) on pacing rate is a fundamental property of cardiac myocytes that, when altered, may promote life-threatening cardiac arrhythmias. We have developed a detailed and physiologically based mathematical canine ventricular cell model (Hund-Rudy dynamic [HRd] cell model) that simulates rate-dependent phenomena associated with ion-channel kinetics, AP properties, and Ca handling. The dog is commonly used to investigate cardiac electrophysiology, making it a logical choice for modeling. An epicardial myocyte was chosen rather than endocardial or midmyocardial myocytes because epicardial cells contain the highest density of I_{to1} (transient outward K^+ current), producing a unique and complex AP morphology.

Ca^{2+}/calmodulin-dependent protein kinase[1] (CaMKII) mediates an important regulatory pathway in myocytes.[2] On activation by Ca^{2+}/calmodulin, CaMKII phosphorylates neighboring subunits (autophosphorylation), which enables detection of Ca^{2+} spike frequency.[3] In cardiomyocytes, CaMKII substrates include L-type Ca^{2+} channels (LTCCs), ryanodine receptor Ca^{2+}-release channels (RyRs), sarcoplasmic reticulum Ca^{2+}-ATPase (SR Ca^{2+}-uptake pump), and phospholamban (PLB).[4–10] This suggests an important role for CaMKII in cardiac Ca^{2+}-handling rate dependence and electrophysiology. We used the HRd model to gain new insights into ionic processes underlying AP and CaT rate dependence and how CaMKII regulates these processes.

Methods

Complete HRd equations, definitions, and detailed comments appear in the online-only Data Supplement. Important model properties (schematic in Figure 1A) are summarized here.

Ca^{2+}/Calmodulin-Dependent Protein Kinase II

The CaMKII formulation was adapted from Hanson et al[3] and responds dynamically to $[Ca^{2+}]_{ss}$ (subspace Ca^{2+} concentration) elevation during the CaT. Kinase subunits can be inactive, in a Ca^{2+}/calmodulin-bound active state ($CaMK_{bound}$), or in a "trapped" state ($CaMK_{trap}$), wherein the subunit remains active for some time after $[Ca^{2+}]_{ss}$ returns to diastolic values. Autophosphorylation of 1 subunit by another promotes transition from $CaMK_{bound}$ to $CaMK_{trap}$. Trapped subunits are dephosphorylated at a constant rate, β_{CaMK}, of 0.00068 ms^{-1}, a moderate value compared with the cycle-length (CL) range investigated here.

Subspace Compartment

The junctional SR membrane abuts the sarcolemma along t-tubules, where LTCC and RyR clusters are localized,[11] creating a subspace in which the Ca^{2+} concentration ($[Ca^{2+}]_{ss}$) rises faster and reaches larger values compared with that of the bulk myoplasm. We modeled the subspace as a compartment into which LTCCs and RyRs open, generating a local Ca^{2+} concentration, $[Ca^{2+}]_{ss}$. Anionic sarcolemmal and SR membrane binding sites act as calcium buffers.[12] The Ca^{2+}-dependent transient outward current (I_{to2}) is a ligand-gated

Received January 29, 2004; de novo received April 19, 2004; accepted June 7, 2004.

From the Departments of Biomedical Engineering (T.J.H., Y.R.) and Pathology (T.J.H.), Washington University, St. Louis, Mo.

An online-only Data Supplement is available at http://www.circulationaha.org

Correspondence to Yoram Rudy, Department of Biomedical Engineering, Washington University, Campus Box 1097, One Brookings Dr, St. Louis, MO 63130-4899. E-mail rudy@wustl.edu

Circulation **is available at http://www.circulationaha.org** **DOI: 10.1161/01.CIR.0000147231.69595.D3**

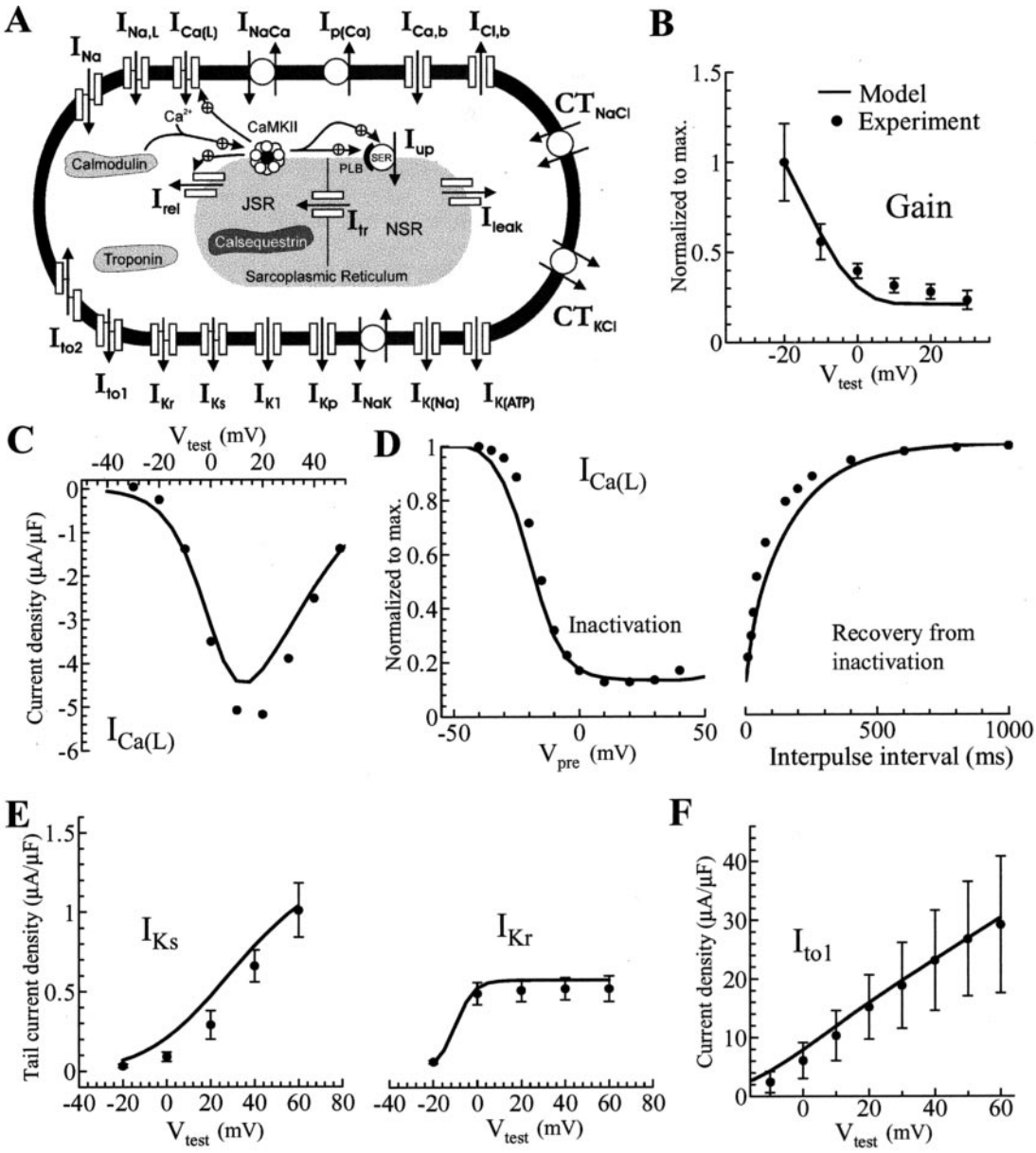

Figure 1. A, Canine ventricular cell model. Symbols are defined in text and in online-only Data Supplement Table I. B, Ratio of peak SR Ca^{2+} release flux to peak LTCC flux vs test potential (V_{test}) in model (line in each panel) and experiment[19] (circles in each panel). Model was clamped for 50 ms to −40 mV holding potential, followed by 50-ms test pulse. C, $I_{Ca(L)}$ I-V relation compared with canine ventricular data.[21] $[Ca^{2+}]_o$=2.0 mmol/L. D, Left, $I_{Ca(L)}$ voltage-dependent inactivation compared with experiment.[21] Variable 1-second prepulse (V_{pre}) was followed by 10-ms holding interval at −50 mV and +80 mV test pulse. Right, $I_{Ca(L)}$ recovery from voltage-dependent inactivation compared with canine ventricular data.[52] Prepulse of 350 ms to +20 mV was followed by varying interpulse interval at −40 mV and +20 mV test pulse. Model Ca^{2+}-dependent inactivation gates were held constant to isolate voltage-dependent inactivation. E, Peak I_{Ks} and I_{Kr} tail currents on repolarization to −40 mV holding potential after 5-second test pulse, compared with canine epicardial data.[24] F, I_{to1} I-V relation compared with canine epicardial data.[27]

Cl^--selective channel. Its low Ca^{2+} sensitivity ($K_{0.5}$=0.1502 mmol/L)[13] supports its incorporation into the Ca^{2+} subspace. CaMKII forms a complex with RyR[14] and is also assumed to be in the subspace.

RyR Ca^{2+}-Release Channel I_{rel}

The I_{rel} formulation includes activation by the L-type Ca^{2+} current, Ca^{2+}-dependent inactivation,[15,16] and open-probability modulation by junctional SR $[Ca^{2+}]$ and $[Ca^{2+}]_{ss}$[17]. Although it is generally accepted that the RyR is regulated by SR Ca^{2+} content[17] and inactivated by cytosolic Ca,[15,16] the relative contribution of each process to SR Ca^{2+}-release termination is unknown. I_{rel} in our formulation terminates via both inactivation and SR regulation of the activation gate.[18] Graded release is achieved by making steady-state activation a continuous function of $I_{Ca(L)}$. Voltage-dependent SR release gain[19] (variable gain, Figure 1B) is introduced through a multiplicative factor dependent on the $I_{Ca(L)}$ driving force.

Though controversial (online-only Data Supplement section J), CaMKII phosphorylation is thought to promote RyR channel opening.[5,14,20] Accordingly, the I_{rel} inactivation time constant (τ_{ri}) depends on CaMKII activity. A 10-ms maximal CaMKII-dependent increase in τ_{ri} yields a steady-state CaT amplitude (CaT_{amp}) 95%[20] greater for control than with CaMKII suppressed at rapid pacing (CL=300 ms).

SR Ca^{2+}-ATPase and PLB

CaMKII phosphorylates the SR,[6] targeting SERCA2a (SR Ca^{2+}-ATPase)[7] and PLB,[8,10] which associates with SERCA2a to inhibit uptake. PLB phosphorylation shifts the Ca^{2+}-binding $K_{0.5}$ and relieves inhibition,[9] whereas direct SERCA2a phosphorylation increases the maximum uptake rate,[7] although this is controversial[9] (online-only Data Supplement section K). and $K_{0.5}$ depend on CaMKII activity to represent this behavior. The maximal CaMKII-dependent increase is 75%,[7] whereas the maximal $K_{0.5}$ decrease is 0.17 μmol/L[9].

L-Type Ca^{2+} Channel

$I_{Ca(L)}$ steady-state activation and current density yield a current-voltage (I-V) relation consistent with canine ventricular data[21] (Figure 1C). The activation variable, d, is raised to a time-dependent and voltage-dependent power (see the online-only Data Supplement). We assume 2 voltage-dependent inactivation gates with steady-state values (Figure 1D) and time constants fitted to canine ventricular data[21,21a] (online-only Data Supplement Figure I). Ca^{2+}-dependent inactivation has a fast process[22] dependent on $[Ca^{2+}]_{ss}$ and LTCC Ca^{2+} entry (approximated as $I_{Ca(L)}$[23]) and a slow process dependent on $I_{Ca(L)}$.[22]

Ca^{2+}-dependent facilitation occurs via CaMKII phosphorylation.[4] The rapid Ca^{2+}-dependent inactivation time constant (τ_{fca}) is CaMKII dependent, producing a maximal 40%[20] increase in peak $I_{Ca(L)}$ relative to the model, with CaMKII suppressed at rapid pacing (CL=500 ms).

Two Components of the Delayed Rectifier K^+ Current

The canine delayed rectifier K^+ current has a rapidly activating component (I_{Kr}) and a slowly activating component (I_{Ks}).[24] The model I_{Ks} has fast (x_{s1}, with time constant τ_{xs1}) and slow (x_{s2}) activation gates. Voltage dependence of τ_{xs1} fits canine data.[24] The slow activation gate is 10 times slower than x_{s1}[24]. I_{Kr} has 1 activation gate, x_r, based on experimental data.[24] I_{Ks} and I_{Kr} conductances were chosen to agree with experimental data[24] (Figure 1E).

Transient Outward K^+ Current

The 4AP-sensitive transient outward K^+ current, I_{to1}, incorporates the activation and inactivation kinetics of Dumaine et al.[25] We add a second inactivation gate with a slower time constant[26] than in Dumaine's formulation. The model I_{to1} I-V curve agrees with experimental data[27] (Figure 1F).

Other Formulations

Cl Homeostasis

I_{to2} inclusion requires modeling intracellular Cl^- regulation by the Na^+-dependent Cl^- cotransporter[28] CT_{NaCl}, the K^+-Cl^- cotransporter[29] CT_{KCl}, and the background Cl^- current $I_{Cl,b}$.

Na^+-Ca^{2+} Exchanger

The Na^+-Ca^{2+} exchanger (I_{NaCa}), from Weber et al,[30] includes an allosteric interaction between intracellular Ca^{2+} and the exchanger.

Late Na^+ Current

Our slowly inactivating late sodium current $I_{Na,L}$[31] formulation uses activation from the Luo-Rudy dynamic (LRd) fast sodium current I_{Na}.[32] Steady-state inactivation and a 600-ms, voltage-independent inactivation time constant were taken from Maltsev et al.[33]

Pacing Studies

The model was paced with a conservative current stimulus[34] (carried by KCl) for 2000 seconds from rest (initial conditions in online-only Data Supplement Table II) at a constant CL. Steady-state APD (at 90% repolarization) and CaT_{amp} (peak systolic $[Ca^{2+}]_i$−minimal diastolic $[Ca^{2+}]_i$) were used to create the APD adaptation curves and the CaT_{amp}-frequency curves, respectively.

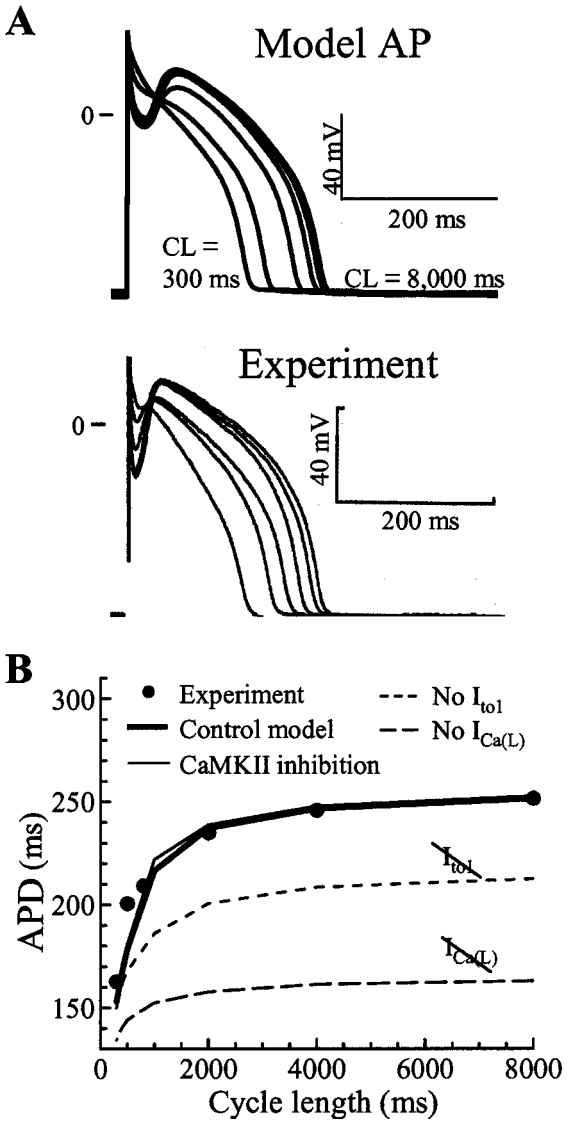

Figure 2. A, Steady-state AP simulated (top) and measured in canine epicardial myocyte[24] (bottom) for CLs of 8000, 4000, 2000, 1000, 500, and 300 ms. B, Steady-state APD vs CL (adaptation curve) in canine epicardial myocyte[26] (circles) and in model under control conditions (bold line), in presence of CaMKII inhibition (thin line), without I_{to1} (dashed line), and without $I_{Ca(L)}$ (long dashed line). Abbreviations are as defined in text.

Results

APD Rate Dependence (Adaptation)

The model AP morphology (Figure 2A) and APD (Figure 2B) agree with canine epicardial recordings[26] over a CL range from 8000 to 300 ms. Most important for canine APD rate adaptation is $I_{Ca(L)}$, supported by the fact that eliminating $I_{Ca(L)}$ from the model reduced adaptation (CL range of 8000 to 300 ms) from 99 to 30 ms (71% decrease, Figure 2B). I_{to1} also plays a role: its elimination reduced adaptation by 38% (Figure 2B). Of secondary importance are I_{NaK} (clamping $[Na^+]_i$ during pacing reduces adaptation by 15%) and $I_{Na,L}$ (eliminating $I_{N,aL}$ reduces adaptation by only 9%). CaMKII inhibition had very little effect on APD adaptation (Figure 2B).

Interestingly, a decrease in the repolarizing current I_{to1} facilitates APD shortening at a fast rate. Comparing steady-

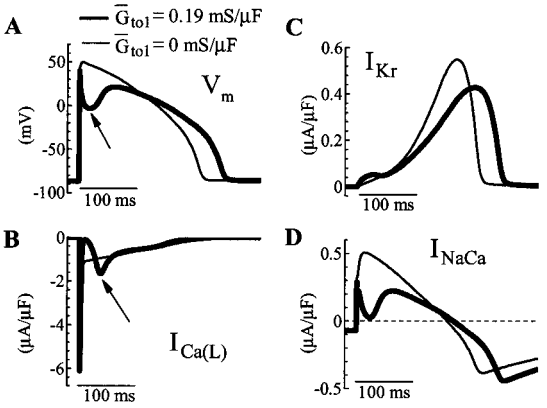

Figure 3. A, AP (arrow identifies rapid phase 1 repolarization); B, $I_{Ca(L)}$ (arrow indicates augmentation); C, I_{Kr}; and D, I_{NaCa} computed for steady-state pacing at CL=8000 ms. Values were computed with (= 0.19 mS/μF, thick line) and without (= 0 mS/μF, thin line) I_{to1}. Abbreviations are as defined in text.

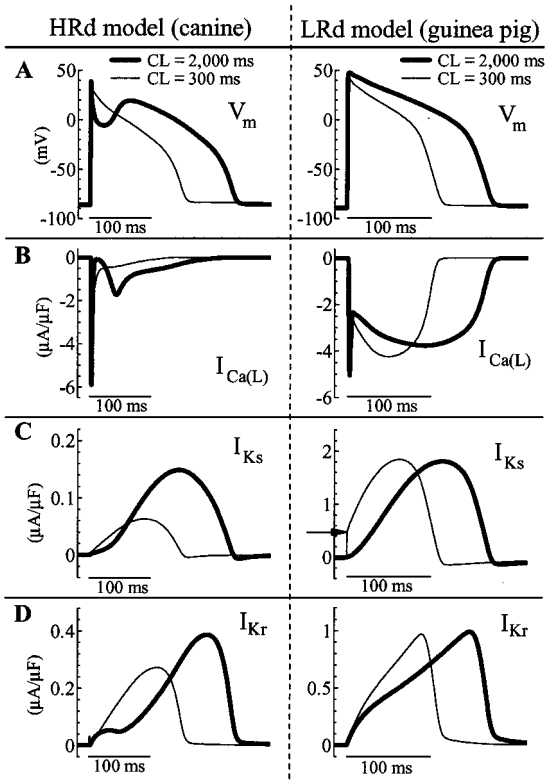

Figure 4. Currents during the AP in HRd canine (left panels) and LRd guinea pig[32] (right panels) cell models. Steady-state values are shown at CLs of 300 ms (thin line) and 2000 ms (thick line). A, AP; B, $I_{Ca(L)}$; C, I_{Ks} (arrow indicates I_{Ks} accumulation); D, I_{Kr}. Abbreviations are as defined in text.

state AP with (=0.19 mS/μF) and without (=0 mS/μF) I_{to1} reveals the effect of I_{to1} on APD (Figure 3). At a slow rate, a large I_{to1} produced a rapid phase 1 repolarization (Figure 3A, arrow) which increased the $I_{Ca(L)}$ driving force and enhanced its voltage-dependent activation during the AP plateau (Figure 3B, arrow). Phase 1 repolarization also increased I_{Kr} activation and decreased the driving force for reverse-mode I_{NaCa}, thus reducing these repolarizing currents (Figure 3C and 3D, respectively). By increasing $I_{Ca(L)}$ and decreasing I_{Kr} and I_{NaCa}, I_{to1} indirectly prolonged APD. During rapid pacing, I_{to1} decreased owing to slow recovery from inactivation, and phase 1 repolarization slowed (Figure 2A). Consequently, indirect APD prolongation by I_{to1} was suppressed at fast pacing rates.

Figure 4 compares rate-dependent changes in AP (Figure 4A) and major ionic currents between the HRd canine model and the LRd guinea pig model.[32] Reduction in $I_{Ca(L)}$ at fast rates was observed in the dog but not in the guinea pig (Figure 4B). Guinea pig adaptation instead is primarily caused by an accumulation of slow deactivating I_{Ks} at fast rates (Figure 4C, arrow).[35] Canine I_{Ks} is small and does not accumulate between beats because of its faster deactivation (Figure 4C). Whereas guinea pig I_{Ks} during the AP was larger than I_{Kr}, canine I_{Kr} is much larger than I_{Ks} (Figure 4C and 4D).

CaT_{amp}-Frequency Relation

Steady-state CaT_{amp} and morphology (Figure 5A), measured[36] and simulated, agreed over a wide pacing range. Consistent with experiment,[36] the model diastolic $[Ca^{2+}]_i$ and CaT_{amp} increased as pacing frequency increased from 0.25 to 2.0 Hz (positive CaT_{amp}-frequency relation, Figure 5B), associated with an increase in simulated CaMKII activity, excitation-contraction coupling (ECC) gain (Figure 5C), and PLB phosphorylation by CaMKII (Figure 5D). CaMKII inhibition produced a negative CaT_{amp}-frequency relation for frequencies >1 Hz (Figure 5B) and flattened the gain-frequency relation (Figure 5C). CaMKII inhibition during pacing (2.0 Hz) (Figure 6) reduced CaT_{amp} (Figure 6B) by decreasing I_{up} (Figure 6C), which reduced SR Ca^{2+} load (Figure 6D) by decreasing peak $I_{Ca(L)}$ (Figure 6E), which reduced the trigger for SR release, and by reducing I_{rel} directly (Figure 6F).

Discussion

We present a dynamic model of the canine ventricular epicardial cell that reproduces experimentally measured AP and CaT over a wide pacing frequency range. Given the broad frequency range during cardiac arrhythmias and the interplay between Ca cycling and cellular electrophysiology in arrhythmogenesis, this model serves as a valuable research tool.

Summary of Important Mechanistic Findings

The major findings of this study are that (1) canine APD adaptation is determined primarily by $I_{Ca(L)}$ reduction at fast rates; (2) I_{to1} contributes to APD adaptation indirectly by augmenting the phase 1 notch at slow rate; (3) ECC gain increases with frequency owing to increased CaMKII activity, producing a positive CaT_{amp}-frequency relation; and (4) CaMKII is important for rate-dependent changes in CaT but does not significantly effect APD adaptation.

Comparison With Existing Models

Canine ventricular AP models have been previously developed to study electrophysiologic remodeling after heart failure[37] and myocardial infarction[38] and APD alternans during rapid pacing.[39] The model presented here distinguishes itself by incorporating (1) dynamic CaMKII activity and regulation of intracellular Ca^{2+} handling; (2) the late Na^+ current, $I_{Na,L}$,

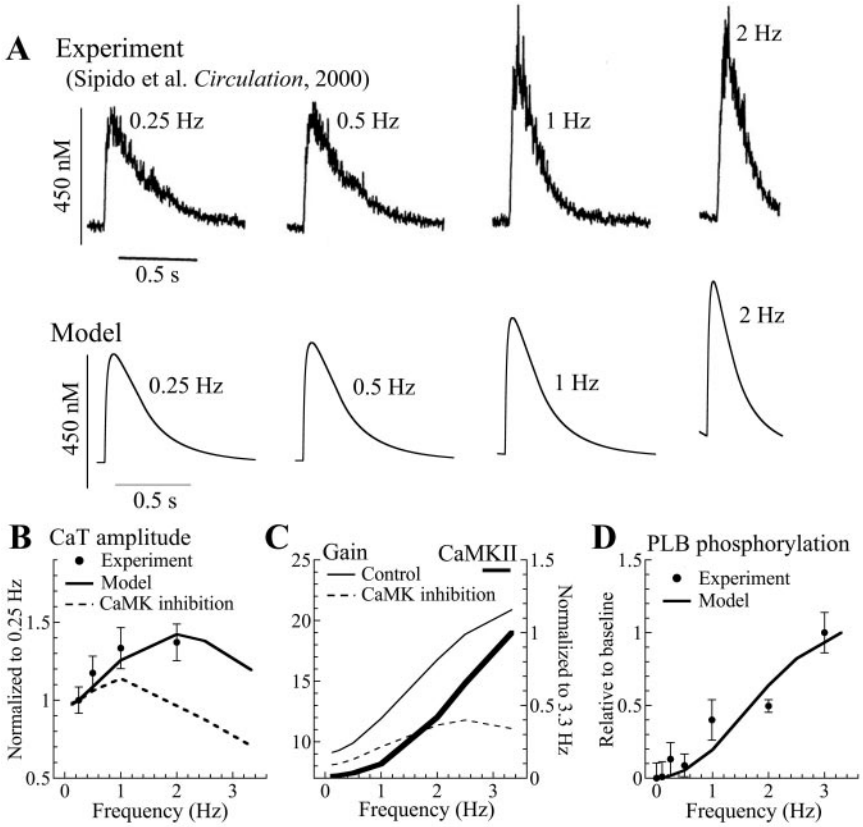

Figure 5. A, Simulated (bottom) and measured[36] (top) steady-state CaT for 0.25-, 0.5-, 1-, and 2-Hz pacing. Adapted from Sipido et al.[36] B, CaT_{amp}-frequency relation for experiment (circles), model under control conditions (line), and in presence of CaMKII inhibition (dashed line). C, Minimal diastolic CaMKII activity (normalized to 3.3 Hz) and ECC gain. ECC gain=, where F_{rel} and $F_{Ca(L)}$ are fluxes through RyRs and LTCCs, respectively, and integration interval, A, equals 1 cycle. Gain is shown for control model (thin line) and in presence of CaMKII inhibition (dashed line). D, PLB phosphorylation vs pacing frequency compared with experimental data.[10] Abbreviations are as defined in text.

and the Ca^{2+}-dependent transient outward current, I_{to2}; (3) dynamic intracellular Cl^- concentration changes; and (4) a novel I_{rel} formulation. Our model represents an important advance in the physiologic representation of rate-dependent cell processes through its inclusion of the CaMKII regulatory pathway, shown experimentally to play a role in the force-frequency relation and rate-dependent CaT abbreviation.[14,20,40]

"Local-control"[41] Ca^{2+} release has been integrated into a canine AP model,[42] wherein SR Ca^{2+} release involves statistical recruitment of individual Ca^{2+} release units. Although this model reproduces macroscopic release based on individual diadic events, computational demands discourage its use in modeling cardiac arrhythmias. Therefore, we reproduced local-control features (variable gain and graded release) by using a macroscopic approach with reduced computational demand.

Effect of CaMKII on Ca^{2+} Handling

We have shown that increased CaMKII activity during rapid pacing augments SR Ca^{2+} release and promotes a positive CaT_{amp}-frequency relation. Our findings are supported by recent experiments measuring increased CaMKII activity and CaMKII-dependent SR Ca^{2+} release after pacing.[14] It is important to note that additional factors determine the CaT_{amp}-frequency relation. Even in the presence of CaMKII inhibition, a positive relation exists over a limited frequency range from 0.125 to 1 Hz (see Figure 5B). Intracellular Na^+ and Ca^{2+} accumulation during rapid pacing produces CaMKII-independent SR loading. Intracellular Ca^{2+} buffer saturation at fast rates also may contribute to a positive force-frequency relation.[43]

APD Adaptation

In the guinea pig, I_{Ks} activates and deactivates more slowly than does I_{Kr}[44]. In the dog, I_{Kr} and I_{Ks} deactivation kinetics are reversed, with I_{Ks} deactivating faster than I_{Kr}.[24] Our simulations suggest that I_{Ks} does not contribute significantly to canine APD adaptation owing to its small amplitude and fast deactivation, consistent with recent canine experiments.[45,46] However, β-adrenergic stimulation enhances I_{Ks},[47] possibly increasing its importance in AP repolarization and adaptation in vivo.

Our results also suggest a role for I_{to1} in determining APD and APD adaptation. Consistent with previous theoretical[48] and experimental[49] studies, we found that I_{to1} creates a phase 1 notch that increases the driving force for $I_{Ca(L)}$ and facilitates activation of a sustained component. In addition, the phase 1 notch decreases the repolarizing currents I_{Kr} and reverse-mode I_{NaCa}. Together, these processes prolong APD. New insight is obtained into the role of I_{to1} in APD adaptation: slow recovery promotes I_{to1} reduction, notch suppression, and less associated APD prolongation at fast rates. Our findings are consistent with greater adaptation in epicardial than in endocardial cells (85 and 65 ms, respectively[26]), which have a greatly diminished I_{to1} density. We also found (not shown) that the notch accelerates the time to peak CaT (62 ms in control vs 83 ms without I_{to1}), consistent with experimental observations.[50]

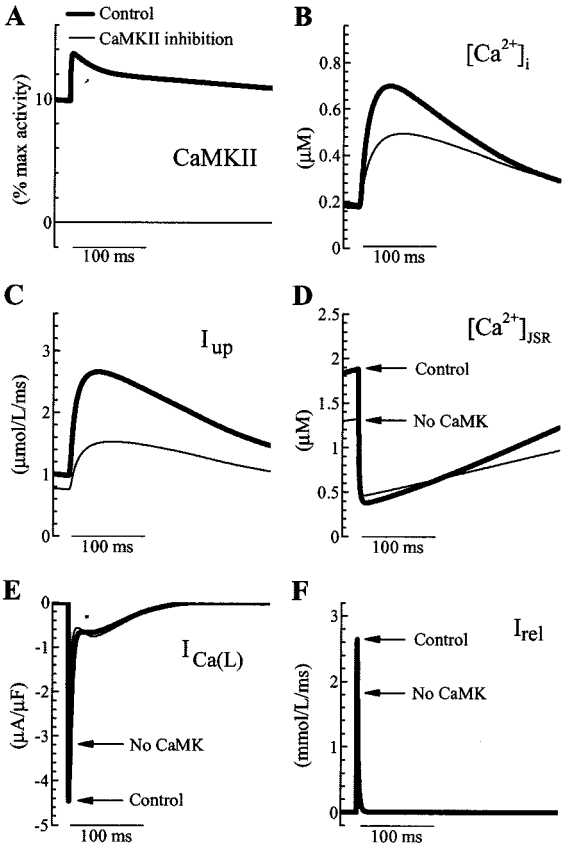

Figure 6. Effect of CaMKII inhibition on CaT. A, CaMKII activity; B, $[Ca^{2+}]_i$; C, I_{up}; D, $[Ca^{2+}]_{JSR}$ (arrows indicate loading); E, $I_{Ca(L)}$ (arrow indicates peak); and F, I_{rel} for steady-state pacing at CL=500 ms (2.0 Hz) in model under control conditions (thick line) and in presence of CaMKII inhibition (thin line). Quantities are shown during AP. Abbreviations are as defined in text.

Limitations

The model formulation was based, wherever possible, on recent experimental data and current understanding of cardiac electrophysiology and Ca^{2+} handling. However, there are controversies regarding CaMKII and its regulatory effects. Disparate findings exist on whether or not CaMKII phosphorylates SERCA2a directly.[7,9] Similarly, conflicting reports exist on CaMKII regulation of RyR activity.[5,20,51,52] These issues remain unresolved (see online-only Data Supplement, sections J and K). We hope that this study will motivate detailed experimental characterization of CaMKII effects on cellular function.

Acknowledgments

This work was funded by grants R01-HL49054 and R37-HL33343 (to Y.R.) from the National Institutes of Health—National Heart, Lung, and Blood Institute, and a Whitaker Foundation Development Award. We thank Greg Faber, Jonathan Silva, and Keith Decker for helpful discussions and Marlene Siegal for administrative assistance.

References

1. Braun AP, Schulman H. The multifunctional calcium/calmodulin-dependent protein kinase: from form to function. *Annu Rev Physiol*. 1995;57:417–445.
2. Maier LS, Bers DM. Calcium, calmodulin, and calcium-calmodulin kinase II: heartbeat to heartbeat and beyond. *J Mol Cell Cardiol*. 2002; 34:919–939.
3. Hanson PI, Meyer T, Stryer L, Schulman H. Dual role of calmodulin in autophosphorylation of multifunctional CaM kinase may underlie decoding of calcium signals. *Neuron*. 1994;12:943–956.
4. Yuan W, Bers DM. Ca-dependent facilitation of cardiac Ca current is due to Ca-calmodulin-dependent protein kinase. *Am J Physiol Heart Circ Physiol*. 1994;267:H982–H993.
5. Witcher DR, Kovacs RJ, Schulman H, Cefali DC, Jones LR. Unique phosphorylation site on the cardiac ryanodine receptor regulates calcium channel activity. *J Biol Chem*. 1991;266:11144–11152.
6. Le Peuch CJ, Haiech J, Demaille JG. Concerted regulation of cardiac sarcoplasmic reticulum calcium transport by cyclic adenosine monophosphate-dependent and calcium/calmodulin-dependent phosphorylations. *Biochemistry*. 1979;18:5150–5157.
7. Toyofuku T, Curotto Kurzydlowski K, Narayanan N, MacLennan DH. Identification of Ser^{38} as the site in cardiac sarcoplasmic reticulum Ca^{2+}-ATPase that is phosphorylated by Ca^{2+}/calmodulin-dependent protein kinase. *J Biol Chem*. 1994;269:26492–26496.
8. Wegener AD, Simmerman HK, Lindemann JP, Jones LR. Phospholamban phosphorylation in intact ventricles: phosphorylation of serine 16 and threonine 17 in response to β-adrenergic stimulation. *J Biol Chem*. 1989;264:11468–11474.
9. Odermatt A, Kurzydlowski K, MacLennan DH. The v_{max} of the Ca^{2+}-ATPase of cardiac sarcoplasmic reticulum (SERCA2a) is not altered by Ca^{2+}/calmodulin-dependent phosphorylation or by interaction with phospholamban. *J Biol Chem*. 1996;271:14206–14213.
10. Hagemann D, Kuschel M, Kuramochi T, Zhu W, Cheng H, Xiao RP. Frequency-encoding Thr^{17} phospholamban phosphorylation is independent of Ser^{16} phosphorylation in cardiac myocytes. *J Biol Chem*. 2000;275:22532–22536.
11. Langer G, Peskoff A. Calcium concentration and movement in the diadic cleft space of the cardiac ventricular cell. *Biophys J*. 1996;70:1169–1182.
12. Smith G, Keizer J, Stern M, Lederer W, Cheng H. A simple numerical model of calcium spark formation and detection in cardiac myocytes. *Biophys J*. 1998;75:15–32.
13. Collier ML, Levesque PC, Kenyon JL, Hume JR. Unitary Cl^- channels activated by cytoplasmic Ca^{2+} in canine ventricular myocytes. *Circ Res*. 1996;78:936–944.
14. Wehrens XH, Lehnart SE, Reiken SR, Marks AR. Ca^{2+}/calmodulin-dependent protein kinase II phosphorylation regulates the cardiac ryanodine receptor. *Circ Res*. 2004;94:e61–e70.
15. Sham J, Song L, Chen Y, Deng L, Stern M, Lakatta E, Cheng H. Termination of Ca^{2+} release by a local inactivation of ryanodine receptors in cardiac myocytes. *Proc Natl Acad Sci U S A*. 1998;95:15096–15101.
16. Fabiato A. Time and calcium dependence of activation and inactivation of calcium-induced release of calcium from the sarcoplasmic reticulum of a skinned canine cardiac Purkinje cell. *J Gen Physiol*. 1985;85:247–289.
17. Lukyanenko V, Gyorke I, Gyorke S. Regulation of calcium release by calcium inside the sarcoplasmic reticulum in ventricular myocytes. *Pflugers Arch*. 1996;432:1047–1054.
18. Shannon TR, Guo T, Bers DM. Ca^{2+} scraps: local depletions of free $[Ca^{2+}]$ in cardiac sarcoplasmic reticulum during contractions leave substantial Ca^{2+} reserve. *Circ Res*. 2003;93:40–45.
19. Wier WG, Egan TM, Lopez Lopez JR, Balke CW. Local control of excitation-contraction coupling in rat heart cells. *J Physiol (Lond)*. 1994; 474:463–471.
20. Li L, Satoh H, Ginsburg KS, Bers DM. The effect of Ca^{2+}-calmodulin-dependent protein kinase II on cardiac excitation-contraction coupling in ferret ventricular myocytes. *J Physiol (Lond)*. 1997;501:17–31.
21. Rubart M, Lopshire JC, Fineberg NS, Zipes DP. Changes in left ventricular repolarization and ion channel currents following a transient rate increase superimposed on bradycardia in anesthetized dogs. *J Cardiovasc Electrophysiol*. 2000;11:652–664.
21a. Aggarwal R, Boyden PA. Diminished Ca^{2+} and Ba^{2+} currents in myocytes surviving in the epicardial border zone of the 5-day infarcted canine heart. *Circ Res*. 1995;77:1180–1191.
22. Sun H, Leblanc N, Nattel S. Mechanisms of inactivation of L-type calcium channels in human atrial myocytes. *Am J Physiol Heart Circ Physiol*. 1997;272:H1625–H1635.
23. Hirano Y, Hiraoka M. Ca^{2+} entry-dependent inactivation of L-type Ca current: a novel formulation for cardiac action potential models. *Biophys J*. 2003;84:696–708.

24. Liu DW, Antzelevitch C. Characteristics of the delayed rectifier current (I_{Kr} and I_{Ks}) in canine ventricular epicardial, midmyocardial, and endocardial myocytes: a weaker I_{Ks} contributes to the longer action potential of the M cell. *Circ Res*. 1995;76:351–365.
25. Dumaine R, Towbin JA, Brugada P, Vatta M, Nesterenko DV, Nesterenko VV, Brugada J, Brugada R, Antzelevitch C. Ionic mechanisms responsible for the electrocardiographic phenotype of the Brugada syndrome are temperature dependent. *Circ Res*. 1999;85:803–809.
26. Liu DW, Gintant GA, Antzelevitch C. Ionic bases for electrophysiological distinctions among epicardial, midmyocardial, and endocardial myocytes from the free wall of the canine left ventricle. *Circ Res*. 1993;72:671–687.
27. Lue WM, Boyden PA. Abnormal electrical properties of myocytes from chronically infarcted canine heart: alterations in V_{max} and the transient outward current. *Circulation*. 1992;85:1175–1188.
28. Kneller J, Ramirez RJ, Chartier D, Courtemanche M, Nattel S. Time-dependent transients in an ionically based mathematical model of the canine atrial action potential. *Am J Physiol Heart Circ Physiol*. 2002; 282:H1437–H1451.
29. Piwnica-Worms D, Jacob R, Horres CR, Lieberman M. Potassium-chloride cotransport in cultured chick heart cells. *Am J Physiol Cell Physiol*. 1985;249:C337–C344.
30. Weber CR, Ginsburg KS, Philipson KD, Shannon TR, Bers DM. Allosteric regulation of Na/Ca exchange current by cytosolic Ca in intact cardiac myocytes. *J Gen Physiol*. 2001;117:119–131.
31. Zygmunt AC, Eddlestone GT, Thomas GP, Nesterenko VV, Antzelevitch C. Larger late sodium conductance in M cells contributes to electrical heterogeneity in canine ventricle. *Am J Physiol Heart Circ Physiol*. 2001;281:H689–H697.
32. Luo CH, Rudy Y. A dynamic model of the cardiac ventricular action potential, I: simulations of ionic currents and concentration changes. *Circ Res*. 1994;74:1071–1096.
33. Maltsev VA, Sabbah HN, Undrovinas AI. Late sodium current is a novel target for amiodarone: studies in failing human myocardium. *J Mol Cell Cardiol*. 2001;33:923–932.
34. Hund TJ, Kucera JP, Otani NF, Rudy Y. Ionic charge conservation and long-term steady state in the Luo-Rudy dynamic model of the cardiac cell. *Biophys J*. 2001;81:3324–3331.
35. Viswanathan P, Shaw R, Rudy Y. Effects of I_{Kr} and I_{Ks} heterogeneity on action potential duration and its rate dependence: a simulation study. *Circulation*. 1999;99:2466–2474.
36. Sipido KR, Volders PG, de Groot SH, Verdonck F, Van de Werf F, Wellens HJ, Vos MA. Enhanced Ca^{2+} release and Na/Ca exchange activity in hypertrophied canine ventricular myocytes: potential link between contractile adaptation and arrhythmogenesis. *Circulation*. 2000; 102:2137–2144.
37. Winslow RL, Rice J, Jafri S, Marbán E, O'Rourke B. Mechanisms of altered excitation-contraction coupling in canine tachycardia-induced heart failure, II: model studies. *Circ Res*. 1999;84:571–586.
38. Cabo C, Boyden P. Electrical remodeling of the epicardial border zone in the canine infarcted heart: a computational analysis. *Am J Physiol Heart Circ Physiol*. 2003;284:H372–H384.
39. Fox JJ, McHarg JL, Gilmour RF Jr. Ionic mechanism of electrical alternans. *Am J Physiol Heart Circ Physiol*. 2002;282:H516–H530.
40. Bassani RA, Mattiazzi A, Bers DM. CaMKII is responsible for activity-dependent acceleration of relaxation in rat ventricular myocytes. *Am J Physiol Heart Circ Physiol*. 1995;268:H703–H712.
41. Stern M. Theory of excitation-contraction coupling in cardiac muscle. *Biophys J*. 1992;63:497–517.
42. Greenstein JL, Winslow RL. An integrative model of the cardiac ventricular myocyte incorporating local control of Ca^{2+} release. *Biophys J*. 2002;83:2918–2945.
43. Kuratomi S, Matsuoka S, Sarai N, Powell T, Noma A. Involvement of Ca^{2+} buffering and Na^{+}/Ca^{2+} exchange in the positive staircase of contraction in guinea-pig ventricular myocytes. *Pflugers Arch*. 2003;446: 347–355.
44. Sanguinetti MC, Jurkiewicz NK. Two components of cardiac delayed rectifier K^{+} current: differential sensitivity to block by class III antiarrhythmic agents. *J Gen Physiol*. 1990;96:195–215.
45. Varro A, Balati B, Iost N, Takacs J, Virag L, Lathrop DA, Csaba L, Talosi L, Papp JG. The role of the delayed rectifier component I_{Ks} in dog ventricular muscle and Purkinje fibre repolarization. *J Physiol (Lond)*. 2000;523:67–81.
46. Stengl M, Volders PG, Thomsen MB, Spatjens RL, Sipido KR, Vos MA. Accumulation of slowly activating delayed rectifier potassium current (I_{Ks}) in canine ventricular myocytes. *J Physiol (Lond)*. 2003;551:777–786.
47. Sanguinetti MC, Jurkiewicz NK, Scott A, Siegl PK. Isoproterenol antagonizes prolongation of refractory period by the class III antiarrhythmic agent E-4031 in guinea pig myocytes: mechanism of action. *Circ Res*. 1991;68:77–84.
48. Greenstein JL, Wu R, Po S, Tomaselli GF, Winslow RL. Role of the calcium-independent transient outward current I_{to1} in shaping action potential morphology and duration. *Circ Res*. 2000;87:1026–1033.
49. Banyasz T, Fulop L, Magyar J, Szentandrassy N, Varro A, Nanasi PP. Endocardial versus epicardial differences in L-type calcium current in canine ventricular myocytes studied by action potential voltage clamp. *Cardiovasc Res*. 2003;58:66–75.
50. Cordeiro JM, Greene L, Heilmann C, Antzelevitch D, Antzelevitch C. Transmural heterogeneity of calcium activity and mechanical function in the canine left ventricle. *Am J Physiol Heart Circ Physiol*. 2004;286: H1471–H1479.
51. Lokuta AJ, Rogers TB, Lederer WJ, Valdivia HH. Modulation of cardiac ryanodine receptors of swine and rabbit by a phosphorylation-dephosphorylation mechanism. *J Physiol (Lond)*. 1995;487:609–622.

Rate Dependence and Regulation of Action Potential and Calcium Transient in a Canine Cardiac Ventricular Cell Model

Thomas J. Hund and Yoram Rudy

Circulation. 2004;110:3168-3174; originally published online October 25, 2004;
doi: 10.1161/01.CIR.0000147231.69595.D3
Circulation is published by the American Heart Association, 7272 Greenville Avenue, Dallas, TX 75231

Print ISSN: 0009-7322. Online ISSN: 1524-4539

TABLE E1: Definitions and abbreviations

I_{Na}	Fast Na^+ current, μA/μF
$I_{Na,L}$	Slowly inactivating late Na^+ current, μA/μF
$I_{Ca(L)}$	Ca^{2+} current through the L-type Ca^{2+} channel, μA/μF
$I_{Ca,Na}$	Na^+ current through the L-type Ca^{2+} channel, μA/μF
$I_{Ca,K}$	K^+ current through the L-type Ca^{2+} channel, μA/μF
I_{Kr}	Rapid delayed rectifier K^+ current, μA/μF
I_{Ks}	Slow delayed rectifier K^+ current, μA/μF
I_{to1}	4AP-sensitive transient outward K^+ current, μA/μF
I_{to2}	Ca^{2+}-dependent transient outward Cl^- current, μA/μF
I_{K1}	Time-independent K^+ current, μA/μF
I_{Kp}	Plateau K^+ current, μA/μF
I_{NaCa}	Na^+-Ca^{2+} exchanger, μA/μF
Allo	Ca^{2+}-dependent allosteric activation factor of I_{NaCa}
ν_{max}	Maxmimal flux of I_{NaCa}, μA/μF
k_{sat}	Saturation factor of I_{NaCa} at negative potentials
η	Position of energy barrier of I_{NaCa}
I_{NaK}	Na^+-K^+ pump, μA/μF
f_{NaK}	Voltage-dependent parameter of I_{NaK}
σ	$[Na^+]_o$-dependent factor of f_{NaK}
$I_{p,Ca}$	Sarcolemmal Ca^{2+} pump, μA/μF
$I_{Ca,b}$	Background Ca^{2+} current, μA/μF
CT_{NaCl}	Na^+-Cl^- cotransporter, mmol/L per ms
CT_{KCl}	K^+-Cl^- cotransporter, mmol/L per ms
SR	Sarcoplasmic reticulum
JSR	Junctional SR
NSR	Network SR
SS	Ca^{2+} subspace
I_{rel}	Ca^{2+} release from JSR to myoplasm, mmol/L per ms
τ_{ri}	Time constant of I_{rel} inactivation, ms
I_{up}	Ca^{2+} uptake from myoplasm to NSR, mmol/L per ms
I_{leak}	Ca^{2+} leak from JSR to myoplasm, mmol/L per ms
I_{tr}	Ca^{2+} transfer from NSR to JSR, mmol/L per ms
τ_{tr}	Time constant of Ca^{2+} transfer from NSR to JSR, ms
I_{diff}	Ca^{2+} transfer from SS to myoplasm, mmol/L per ms
τ_{diff}	Time constant of Ca^{2+} transfer from SS to myoplasm, ms

$I_{Ca,t}$	Total transmembrane Ca^{2+} current, $I_{Ca,t} = I_{Ca(L)} + I_{Ca,b} + I_{p,Ca} - 2I_{NaCa}$
$I_{Na,t}$	Total transmembrane Na^{+} current, $I_{Na,t} = I_{Na} + 3I_{NaK} + I_{Ca,Na} + 3I_{NaCa} + I_{Na,L}$
$I_{K,t}$	Total transmembrane K^{+} current, $I_{K,t} = I_{Ks} + I_{Kr} + I_{K1} + I_{Ca,K} + I_{to1} + I_{Kp} - 2I_{NaK}$
$I_{Cl,t}$	Total transmembrane Cl^{-} current, $I_{Cl,t} = It_{o2} + I_{Cl,b}$
I_{tot}	Total transmembrane current, $I_{tot} = I_{Ca,t} + I_{Na,t} + I_{K,t} + I_{Cl,t}$
I_{stim}	Stimulus current, μA/μF
$CaMK_{bound}$	Fraction of CaMKII binding sites bound to Ca^{2+}/calmodulin
$CaMK_{active}$	Fraction of active CaMKII binding sites.
$CaMK_{trap}$	Fraction of autonomous CaMKII binding sites with trapped calmodulin.
$CaMK_o$	Fraction of active CaMKII binding sites at equilibrium.
α_{CaMK}, β_{CaMK}	Phosphorylation and dephosphorylation rates of CaMKII, respectively, ms^{-1}
ΔP_{CaMK}	CaMKII-dependent factor of substrate parameter P
$\overline{\Delta P}$	Maximal CaMKII-dependent change in substrate parameter P
APD	Action potential duration measured at 90% repolarization
CaT	Calcium transient
CaT_{amp}	Calcium transient amplitude
PLB	Phospholamban
RyR	Ryanodine receptor SR Ca^{2+} release channel
LTCC	L-type Ca^{2+} channel
$\overline{G}_x$	Maximum conductance of channel x, mS/μF
K_m	Half-saturation concentration, mmol/L
m, h, and j	Activation gate, fast inactivation gate, and slow inactivation gate of I_{Na}, respectively
m_L and h_L	Activation gate and inactivation gate of $I_{Na,L}$, respectively
d, f, and f_2	Activation gate, fast voltage-dependent inactivation gate, and slow voltage-dependent inactivation gate of $I_{Ca(L)}$, respectively
pow	Power applied to *d*
f_{Ca} and f_{Ca2}	Fast Ca^{2+}-dependent inactivation gate and slow Ca^{2+}-dependent inactivation gate of $I_{Ca(L)}$, respectively.
X_{s1} and X_{s2}	Fast activation gate and slow activation gate of I_{Ks}, respectively
X_r	Activation gate of I_{Kr}
R_{Kr}	Time-independent rectification gate of I_{Kr}
K_1	Inactivation gate of I_{K1}

a, i, i_2	Activation gate, fast inactivation gate, and slow inactivation gate of I_{to1}, respectively
R_{to1}	Time-independent rectification gate of I_{to1}
aa	Ca^{2+}-dependent activation gate of I_{to2}
ro and ri	Activation gate and inactivation gate of I_{rel}, respectively.
$\Delta ro_{\infty,JSR}$	Modulation of ro_∞ by $[Ca^{2+}]_{JSR}$
vg	Variable gain factor for I_{rel}
y_∞	Steady-state value of gate y
α_y and β_y	Opening and closing rate constants of gate y, respectively, ms^{-1}
τ_y	Time constant of gate y, ms
csqn	Calsequestrin, Ca^{2+} buffer in JSR
trpn	Troponin, Ca^{2+} buffer in myoplasm
cmdn	Calmodulin, Ca^{2+} buffer in myoplasm
BSR	Anionic SR binding sites for Ca^{2+} in SS
BSL	Anionic sarcolemmal binding sites for Ca^{2+} in SS
P_S	Membrane permeability to ion S, cm/s
$P_{S,A}$	Permeability ratio of ion S to ion A
γ_S	Activity coefficient of ion S
$\bar{I}_x$	Maximum current carried through channel x, μA/μF
V_m	Transmembrane potential, mV
z_s	Valence of ion S
C_m	Total cellular membrane capacitance, 1 μF
A_{Cap}	Capacitive membrane area, cm^2
A_{Geo}	Geometric membrane area, cm^2
R_{CG}	Ratio of A_{Cap} to A_{Geo} = 2
E_x	Reversal potential of current x, mV
$[S]_o$ and $[S]_i$	Extracellular and intracellular concentrations of ion S, respectively, mmol/L
$[Ca^{2+}]_{JSR}$	Ca^{2+} concentration in JSR, mmol/L
$[Ca^{2+}]_{NSR}$	Ca^{2+} concentration in NSR, mmol/L
$[Ca^{2+}]_{ss}$	Ca^{2+} concentration in subspace, mmol/L
$[Ca^{2+}]_{i,t}$	Concentration of free and buffered intracellular Ca^{2+}, mmol/L
$\Delta[S]_x$	Change in concentration of ion S in compartment x during one time step, mmol/L
V_x	Volume of compartment x, μL.
F	Faraday constant, 96,487 C/mol
R	Gas constant, 8314 J/kmol/K
T	Temperature, 310 °K

TABLE E2: Ionic concentrations at rest*

$[Ca^{2+}]_i$	0.0822×10^{-3} mmol/L
$[Cl^-]_i$	19.53 mmol/L
$[K^+]_i$	142.82 mmol/L
$[Na^+]_i$	9.71 mmol/L
$[Ca^{2+}]_{JSR}$	1.25 mmol/L
$[Ca^{2+}]_{NSR}$	1.25 mmol/L
$[Ca^{2+}]_o$	1.8 mmol/L
$[Cl^-]_o$	100 mmol/L
$[K^+]_o$	5.4 mmol/L
$[Na^+]_o$	140 mmol/L

***After model is undisturbed for 1000 s.

MODEL EQUATIONS

This section contains complete HRd model equations.

A. CaMKII

We assume saturation of CaMKII by calmodulin and a half-maximal activation of the kinase ($K_{m,CaM}$) at 1.5×10^{-3} mmol/L free Ca^{2+} (values between 0.7×10^{-3} and 4.0×10^{-3} mmol/L free Ca^{2+} have been cited in the literature[1,2]). We use phosphorylation and dephosphorylation rates an order of magnitude faster than those in the Hanson model to agree with the higher activity of δ_B, a common isoform in the heart, than isoforms in the brain[3].

$$CaMK_{bound} = CaMK_o \cdot \left(1 - CaMK_{trap}\right) \cdot \frac{1}{1 + \frac{K_{m,CaM}}{[Ca^{2+}]_{ss}}}$$

$$\frac{dCaMK_{trap}}{dt} = \alpha_{CaMK} \cdot CaMK_{bound} \cdot \left(CaMK_{bound} + CaMK_{trap}\right) - \beta_{CaMK} \cdot CaMK_{trap}$$

$$CaMK_{active} = CaMK_{bound} + CaMK_{trap}$$

$$\alpha_{CaMK} = 0.05 \text{ ms}^{-1};\ \beta_{CaMK} = 0.00068 \text{ ms}^{-1}$$

$$CaMK_o = 0.05;\ K_{m,CaM} = 0.0015 \text{ mmol/L}$$

The CaMKII dependence of a substrate parameter, P, is defined by ΔP_{CaMK}. We assume a half-saturation coefficient $K_{m,CaMK}$ of 0.15 to yield an almost-linear dependence on pacing frequency for frequencies up to 3 Hz[4].

$$\Delta P_{CaMK} = \bar{\Delta}P \cdot \frac{CaMK_{active}}{K_{m,CaMK} + CaMK_{active}}$$

$$K_{m,CaMK} = 0.15$$

$\bar{\Delta}P$ is the maximal CaMKII-dependent change for substrate parameter, P

for $I_{Ca(L)}$,

$$\bar{\Delta}\tau_{fca,CaMK} = 10 \text{ ms}$$

for I_{rel},

$$\bar{\Delta}t_{rel,CaMK} = 10 \text{ ms}$$

for I_{up},

$$\bar{\Delta}I_{up,CaMK} = 0.75;\ \bar{\Delta}K_{m,PLB} = 0.00017 \text{ mmol/L}$$

B. $I_{Ca(L)}$

Steady-state activation and the current density of $I_{Ca(L)}$ are adjusted to agree with the current-voltage relationship measured in canine ventricular myocytes[5]. The formulation for the time constant of activation, τ_d, is modified from Miyoshi et al[6]. $I_{Ca(L)}$ is facilitated by a number of mechanisms, including Ca^{2+}-dependent (via CaMKII, see below) and voltage-dependent pathways[7]. A relatively slow (τ = 130 ms) voltage-dependent facilitation mediated by PKA has been observed in cardiac LTCC[8]. More recently, a fast voltage-dependent facilitation that does not require PKA phosphorylation has been documented in HEK-293 cells expressing the α-

subunit and β-subunit of the cardiac LTCC[9]. The facilitation process in this case has been attributed to intrinsic channel gating with τ = 10 ms[9]. We incorporate fast voltage-dependent facilitation into the model by raising the activation gate, d, to a power which is a function of voltage and time (τ_{pow} = 10 ms[9]). Without this modification, I_{to1} significantly increases peak $I_{Ca(L)}$ (see previous canine models[10,11]) which disagrees with AP voltage-clamp experiments in canine ventricular myocytes[12,13]. Two voltage-dependent inactivation gates are included with steady-state values and time constants fitted to experimental data measured in canine ventricular myocytes[5] (Figure E1). Ca^{2+}-dependent inactivation consists of a fast and a slow process. Consistent with experimental observations[14], steady-state inactivation of the fast process is a function of $[Ca^{2+}]_{ss}$ and $I_{Ca(L)}$[15], while the slow process depends on $I_{Ca(L)}$.

Experiments indicate that CaMKII phosphorylation increases $I_{Ca(L)}$ by between 40% and 50% at rapid pacing[16,17]. We make τ_{fca} dependent on CaMKII to incorporate CaMKII-dependent facilitation[18,19] into the model with a maximal change that produces a 40% facilitation of the peak current at a pacing frequency of 2.0 Hz.

$$I_{Ca(L)} = d^{pow} \cdot f_{ca} \cdot f_{ca2} \cdot f \cdot f_2 \cdot \bar{I}_{Ca}$$

$$\bar{I}_{Ca(L)} = P_{Ca} \cdot z_{Ca}^2 \cdot \frac{(V_m - 15.0) \cdot F^2}{RT} \cdot \frac{\gamma_{Cai} \cdot [Ca]_{ss} \cdot \exp\left(z_{Ca} \cdot (V_m - 15.0) \cdot F / (RT)\right) - \gamma_{Cao} \cdot [Ca]_o}{\exp\left(z_{Ca} (V_m - 15.0) \cdot F / (RT)\right) - 1}$$

$$d_\infty = \frac{1}{1 + \exp\left(-(V_m - 4)/6.74\right)}$$

$$\tau_d = 0.59 + 0.8 \cdot \frac{\exp\left(0.052 \cdot (V_m + 13)\right)}{1 + \exp\left(0.132 \cdot (V_m + 13)\right)}$$

$$pow_\infty = 9 - \frac{8}{1 + \exp\left(-(V_m + 65)/3.4\right)}$$

$$\tau_{pow} = 10.0 \text{ ms}$$

$$f_\infty = \frac{0.7}{1.0 + \exp\left((V_m + 17.12)/7\right)} + 0.3$$

$$f_{2\infty} = \frac{0.77}{1.0 + \exp\left((V_m + 17.12)/7\right)} + 0.23$$

$$\tau_f = \frac{1}{0.2411 \cdot \exp\left(-\left[0.045 \cdot (V_m - 9.6914)\right] \cdot \left[0.045 \cdot (V_m - 9.6914)\right]\right) + 0.0529}$$

$$\tau_{f2} = \frac{1}{0.0423 \cdot \exp\left(-\left[0.059 \cdot (V_m - 18.5726)\right] \cdot \left[0.059 \cdot (V_m - 18.5726)\right]\right) + 0.0054}$$

$$f_{Ca,\infty} = \frac{0.3}{1 - \frac{I_{Ca(L)}}{0.05}} + \frac{0.55}{1 + \frac{[Ca^{2+}]_{ss}}{0.003}} + 0.15$$

$$f_{Ca2,\infty} = \frac{1}{1 - \frac{I_{Ca(L)}}{0.01}}$$

$$\Delta\tau_{fca,CaMK} = \overline{\Delta\tau}_{fca,CaMK} \cdot \frac{CaMK_{active}}{K_{m,CaMK} + CaMK_{active}}$$

$$\overline{\Delta\tau}_{fca,CaMK} = 10 \text{ ms}$$

$$\tau_{fca} = \Delta\tau_{fca,CaMK} + 0.5 + \frac{1}{1.0 + [Ca^{2+}]_{ss}/0.003} \text{ ms}$$

$$\tau_{fca2} = \frac{300.0}{1 + \exp\left(\left[-I_{Ca(L)} - 0.175\right]/0.04\right)} + 125.0$$

$$K_{m,CaMK} = 0.15$$

$P_{Ca} = 2.43\times10^{-4}$ cm/s; $\gamma_{Cai} = 1$; $\gamma_{Cao} = 0.341$

C. I_{Ks}

I_{Ks} has a fast activation gate (x_{s1}) and a slow activation gate (x_{s2})[20]. The voltage-dependence of the time constant of activation, τ_{Xs1}, is fit to data from the canine[20]. The conductance is scaled to fit tail currents from canine epicardial cells[20].

$$\overline{G}_{Ks} = 0.0248975\left(1 + \frac{0.6}{1 + \left(3.8\times10^{-5}/[Ca^{2+}]_i\right)^{1.4}}\right)$$

$$E_{Ks} = \frac{RT}{F} \cdot \ln\left(\frac{[K^+]_o + P_{Na,K}\cdot[Na^+]_o}{[K^+]_i + P_{Na,K}\cdot[Na^+]_i}\right)$$

$$X_{s\infty} = X_{s2\infty} = \frac{1}{1 + \exp\left(-(V_m - 10.5)/24.7\right)}$$

$$\tau_{xs1} = \frac{1}{\frac{7.61\times10^{-5}\cdot(V_m + 44.6)}{1 - \exp\left(-9.97(V_m + 44.6)\right)} + \frac{3.6\times10^{-4}\cdot(V_m - 0.55)}{\exp\left(0.128\cdot(V_m - 0.55)\right) - 1}}$$

$$\tau_{Xs2} = 2\cdot\tau_{Xs1}$$

$$P_{Na,K} = 0.01833$$

$$I_{Ks} = \overline{G}_{Ks}\cdot X_s \cdot X_{S2}\cdot(V_m - E_{Ks})$$

D. I_{Kr}

The time constant of activation, τ_{Xr}, is fit to data from the canine[20]. The conductance is scaled according to data from the canine[20].

$$\overline{G}_{Kr} = 0.0138542\cdot\sqrt{\frac{[K^+]_o}{5.4}}$$

$$E_{Kr} = \frac{RT}{F}\cdot\ln\left(\frac{[K^+]_o}{[K^+]_i}\right)$$

$$\tau_{Xr} = \frac{1}{\frac{0.6\times10^{-3}\cdot(V_m - 1.7384)}{1-\exp\left(-0.136\cdot(V_m-1.7384)\right)} + \frac{3\times10^{-4}\cdot(V_m+38.3608)}{\exp\left(0.1522\cdot(V_m+38.3608)\right)-1}}$$

$$X_{r\infty} = \frac{1}{1+\exp\left(-(V_m+10.085)/4.25\right)}$$

$$R_{Kr} = \frac{1}{1+\exp\left((V_m+10)/15.4\right)}$$

$$I_{Kr} = \overline{G}_{Kr}\cdot X_r \cdot R_{Kr}\cdot(V_m - E_{Kr})$$

E. I_{to1}

The conductance of I_{to1} is chosen to agree with measurements in canine epicardial myocytes[21]. A second inactivation gate is included to account for the slow recovery from inactivation measured in the canine[22].

$$E_{to1} = \frac{RT}{F}\cdot\ln\left(\frac{[K^+]_o}{[K^+]_i}\right)$$

$$R_{to1} = \exp\left(V_m/300\right)$$

$$\alpha_a = \frac{25\cdot\exp\left((V_m-40)/25\right)}{1+\exp\left((V_m-40)/25\right)}$$

$$\beta_a = \frac{25\cdot\exp\left(-(V_m+90)/25\right)}{1+\exp\left(-(V_m+90)/25\right)}$$

$$\alpha_i = \frac{0.03}{1+\exp\left((V_m+60)/5\right)}$$

$$\beta_i = \frac{0.2\cdot\exp\left((V_m+25)/5\right)}{1+\exp\left((V_m+25)/5\right)}$$

$$\alpha_{i2} = \frac{0.00225}{1+\exp\left((V_m+60)/5\right)}$$

$$\beta_{i2} = \frac{0.1\cdot\exp\left((V_m+25)/5\right)}{1+\exp\left((V_m+25)/5\right)}$$

$$\overline{G}_{to1} = 0.19 \text{ mS/}\mu\text{F}$$

$$I_{to1} = \overline{G}_{to1}\cdot a^3\cdot i\cdot i_2\cdot R_{to1}\cdot(V_m - E_{to1})$$

F. I_{NaCa}

In our model, we use the formulation of Weber et al. that includes allosteric activation by $[Ca^{2+}]_i$[23]. We scale $[Ca^{2+}]_i$ by a factor of 1.5 to approximate higher $[Ca^{2+}]_i$ seen by the exchanger[24].

$$I_{NaCa} = Allo \cdot \Delta E$$

$$Allo = \frac{1}{1 + \left(\frac{K_{mCa,act}}{1.5 \cdot [Ca^{2+}]_i} \right)^2}$$

$$\Delta E = \frac{v_{\max} \cdot \left([Na^+]_i^3 \cdot [Ca^{2+}]_o \cdot \exp\left(\eta \cdot \frac{VF}{RT} \right) - [Na^+]_o^3 \cdot 1.5 \cdot [Ca^{2+}]_i \cdot \exp\left(\frac{(\eta - 1) \cdot VF}{RT} \right) \right)}{\left(1 + k_{sat} \exp\left(\frac{(\eta - 1) \cdot VF}{RT} \right) \right) \cdot \left(\begin{array}{l} K_{m,Cao}[Na^+]_i^3 + K_{m,Nao}^3 \cdot 1.5 \cdot [Ca^{2+}]_i + K_{m,Nai}^3 \cdot [Ca^{2+}]_o \cdot \left(1 + \frac{1.5 \cdot [Ca^{2+}]_i}{K_{m,Cai}} \right) \\ + K_{m,Cai} \cdot [Na^+]_o^3 \cdot \left(1 + \frac{[Na^+]_i^3}{K_{m,Nai}^3} \right) + [Na^+]_i^3 \cdot [Ca^{2+}]_o + [Na^+]_o^3 \cdot 1.5 \cdot [Ca^{2+}]_i \end{array} \right)}$$

$v_{\max} = 4.5\ \mu A/\mu F$; $k_{sat} = 0.27$; $\eta = 0.35$
$K_{m,Nai} = 12.3$ mmol/L; $K_{m,Nao} = 87.5$ mmol/L
$K_{m,Cai} = 0.0036$ mmol/L; $K_{m,Cao} = 1.3$ mmol/L
$K_{mCa,act} = 1.25 \times 10^{-4}$ mmol/L

G. I_{Na}

Our formulation is the same as that in the Luo-Rudy model[25] with a reduced conductance.

$$\overline{G}_{Na} = 8.25\ \text{mS}/\mu\text{F}$$

$$E_{Na} = \frac{RT}{F} \cdot \ln\left(\frac{[Na^+]_o}{[Na^+]_i} \right)$$

$$\alpha_m = \frac{0.32 \cdot (V_m + 47.13)}{1 - \exp(-0.1 \cdot (V_m + 47.13))}$$

$$\beta_m = 0.08 \cdot \exp\left(-\frac{V_m}{11} \right)$$

If $V_m \geq -40.0$ mV,

$$\alpha_h = 0.0$$

$$\beta_h = \frac{1}{0.13 \cdot \left(1 + \exp\left(\frac{V_m + 10.66}{-11.1} \right) \right)}$$

$$\alpha_j = 0.0$$

$$\beta_j = \frac{0.3 \cdot \left(-2.535 \times 10^{-7}\right) \cdot V_m}{\exp\left(-0.1 \cdot \left(V_m + 32\right)\right) + 1}$$

else

$$\alpha_h = 0.135 \cdot \exp\left(\frac{\left(80.0 + V_m\right)}{-6.8}\right)$$

$$\beta_h = 3.56 \cdot \exp\left(0.079 \cdot V_m\right) + 3.1 \times 10^5 \cdot \exp\left(0.35 \cdot V_m\right)$$

$$\alpha_j = \frac{\left(-1.2714 \times 10^5 \cdot \exp\left(0.2444 \cdot V_m\right) - 3.474 \times 10^{-5} \cdot \exp\left(-0.04391 \cdot V_m\right)\right) \cdot \left(V_m + 37.78\right)}{1 + \exp\left(0.311 \cdot \left(V_m + 79.23\right)\right)}$$

$$\beta_j = \frac{0.1212 \cdot \exp\left(-0.01052 \cdot V_m\right)}{1 + \exp\left(-0.1378 \cdot \left(V_m + 40.14\right)\right)}$$

$$I_{Na} = \overline{G}_{Na} \cdot m^3 \cdot h \cdot j \cdot \left(V_m - E_{Na}\right)$$

H. $I_{Na,L}$

For activation of $I_{Na,L}$, we use the kinetics and steady-state voltage dependence of I_{Na} from the original LRd model[25]. The voltage dependence and kinetics of inactivation are based on data from human ventricular myocytes[26]. The conductance yields a current density of 0.3 μA/μF in response to a 295 ms pulse to 0 mV after a 2000 ms clamp to -130 mV to relieve inactivation (0.46 ± 0.068 pA/pF measured in canine epicardial myocytes[27]).

$$E_{Na,L} = \frac{RT}{F} \cdot \ln\left(\frac{[Na^+]_o}{[Na^+]_i}\right)$$

$$\alpha_{m,L} = \frac{0.32 \cdot \left(V_m + 47.13\right)}{1 - \exp\left(-0.1 \cdot \left(V_m + 47.13\right)\right)}$$

$$\beta_{m,L} = 0.08 \cdot \exp\left(\frac{-V_m}{11.0}\right)$$

$$h_{L,\infty} = \frac{1}{1 + \exp\left(\left(V_m + 91\right)/6.1\right)}$$

$\tau_{hL} = 600$ ms

$\overline{G}_{Na,L} = 0.0065$ mS/μF

$$I_{Na,L} = \overline{G}_{Na,L} \cdot m_L^3 \cdot h_L \cdot \left(V_m - E_{Na,L}\right)$$

I. Cl^- currents

Our model of Cl^- regulation follows that suggested by Baumgarten et al.[28] and includes the Na^+-dependent Cl^- cotransporter[29], CT_{NaCl}, the K^+-Cl^- cotransporter[30], CT_{KCl}, and a background Cl^- current, $I_{Cl,b}$. $[Cl^-]_o$ = 100 mmol/L[28] and resting [Cl-]i = 19 mmol/L (Table 2).

$$E_{Cl} = -\frac{RT}{F}\cdot\ln\left(\frac{[Cl^-]_o}{[Cl^-]_i}\right)$$

$$E_K = \frac{RT}{F}\cdot\ln\left(\frac{[K^+]_o}{[K^+]_i}\right)$$

$$E_{Na} = \frac{RT}{F}\cdot\ln\left(\frac{[Na^+]_o}{[Na^+]_i}\right)$$

a. K^+-Cl^- cotransporter, CT_{KCl}

$$CT_{KCl} = \overline{CT}_{KCl}\cdot\frac{(E_K - E_{Cl})}{(E_K - E_{Cl}) + 87.8251}$$

$$\overline{CT}_{KCl} = 7.0756\times10^{-6}\ \text{mmol/L per ms}$$

b. Na^+-Cl^- cotransporter, CT_{NaCl}

$$CT_{NaCl} = \overline{CT}_{NaCl}\cdot\frac{\left(E_{Na} - E_{Cl}\right)^4}{\left(E_{Na} - E_{Cl}\right)^4 + 87.8251^4}$$

$$\overline{CT}_{NaCl} = 9.8443\times10^{-6}\ \text{mmol/L per ms}$$

The formulation for CT_{NaCl} comes from [29]. $\overline{CT}_{NaCl} = 9.8443\times10^{-6}$ mmol/ms yields a resting Cl^- uptake rate of 7.1×10^{-6} mmol/ms, close to the value of 8×10^{-6} mmol/ms measured experimentally[28].

c. Cl^- background current, I_{Clb}

$$\overline{G}_{Cl,b} = 2.25\times10^{-4}\ \mu\text{A}/\mu\text{F}$$

$$I_{Cl,b} = \overline{G}_{Cl,b}\cdot\left(V_m - E_{Cl}\right)$$

d. Ca^{2+}-dependent transient outward current, I_{to2}

I_{to2} is simple ligand gated channel with a very low affinity for Ca^{2+} (K_m = 0.1502 mM [31]). In our model, I_{to2} is assumed to be in the subspace and is therefore a function of $[Ca^{2+}]_{ss}$. Based on the suggestion of Collier et al. we use the constant field equation for I_{to2}[31].

$$\bar{I}_{to2} = P_{Cl}\cdot z_{Cl}^2\cdot\frac{V_m\cdot F^2}{RT}\cdot\frac{[Cl]_i - [Cl]_o\cdot\exp\left(-z_{Cl}\cdot V_m\cdot F/\left(RT\right)\right)}{1-\exp\left(-z_{Cl}\cdot V_m\cdot F/\left(RT\right)\right)}$$

$$aa_{\infty} = \frac{1}{1+\frac{K_{m,to2}}{[Ca^{2+}]_r}}$$

$$\tau_{aa} = 1 \text{ ms}$$

$$P_{cl} = 4.0\times10^{-7} \text{ cm/s}$$

$$K_{m,to2} = 0.1502 \text{ mM}$$

$$I_{to2} = \bar{I}_{to2} \cdot aa$$

J. I_{rel}

Our formulation for I_{rel} includes an $I_{Ca(L)}$-dependent activation gate, a Ca^{2+}-dependent inactivation gate[Sham, 1998 #590;Fabiato, 1985 #800], and modulation of gating by SR Ca^{2+} content[Lukyanenko, 1996 #796;DelPrincipe, 1999 #795]. The dependence of ro_{∞} on $[Ca^{2+}]_{JSR}$, $\Delta ro_{\infty,JSR}$, uses a Hill coefficient of 1.9[Lukyanenko, 1996 #796] with an EC_{50} that depends on $[Ca^{2+}]_{ss}$ (EC_{50} = 2.6 at $[Ca^{2+}]_{ss}$ = 0.1 μM and EC_{50} = 10.6 at $[Ca^{2+}]_{ss}$ = 1.0 μM[Lukyanenko, 1996 #796]).

Studies on canine SR vesicles show that phosphorylation of the RyR by CaMKII activates the channel[37]. While some have found a decrease in RyR activity in response to increased CaMKII activity[38,39], drug studies[40] and studies where the SR calcium content is tightly controlled[16] provide strong evidence for a positive regulation of RyR by CaMKII. Recently, Ser^{2815} has been identified as the unique site on RyR phosphorylated by CaMKII[Wehrens, 2004 #912]. This same group also found an increase in channel open probability in response to CaMKII phosphorylation. Based on these data, we make τ of I_{rel} inactivation a function of CaMKII activity. Maximal CaMKII-dependent increase in τ_{ri} of 10 ms yields a steady-state CaT amplitude (CaT_{amp}) 95% greater for control than for the model with CaMKII suppressed at rapid pacing (CL = 300 ms). This agrees with experiments in ferret ventricular myocytes where control CaT_{amp} is 100% greater than CaT_{amp} in cells treated with KN-93 to suppress CaMKII[16].

$$\bar{\Delta}\tau_{rel,CaMK} = 10 \text{ ms} \; ; \; K_{m,CaMK} = 0.15$$

$$\Delta\tau_{rel,CaMK} = \bar{\Delta}\tau_{rel,CaMK} \cdot \frac{CaMK_{active}}{K_{m,CaMK} + CaMK_{active}}$$

$$\Delta ro_{\infty,JSR} = \frac{[Ca^{2+}]_{JSR}^{1.9}}{[Ca^{2+}]_{JSR}^{1.9} + \left(\frac{49.28\cdot[Ca^{2+}]_{ss}}{[Ca^{2+}]_{ss}+0.0028}\right)^{1.9}}$$

$$ro_{\infty} = \frac{I_{Ca(L)}^{2}}{I_{Ca(L)}^{2}+1.0^{2}} \cdot \Delta ro_{\infty,JSR}$$

$$\tau_{ro} = 3 \text{ ms}$$

$$cafac = \frac{1}{1+\exp\left(\left[I_{Ca(L)}+0.05\right]/0.015\right)}$$

$$ri_{\infty} = \frac{1}{1+\exp\left(\left[\left[Ca^{2+}\right]_{ss} - 0.0004 + 0.002\cdot cafac\right]/0.000025\right)}$$

$$\tau_{ri} = \frac{350 - \Delta\tau_{rel,CaMK}}{1+\exp\left(\left[\left[Ca^{2+}\right]_{ss} - 0.003 + 0.003\cdot cafac\right]/0.0002\right)} + 3 + \Delta\tau_{rel,CaMK} \text{ ms}$$

$$\overline{G}_{rel} = 3000\cdot vg \text{ ms}^{-1}$$

$$vg = \frac{1}{1+\exp\left(\left[\overline{I}_{Ca(L)} + 13\right]/5\right)}$$

$$I_{rel} = \overline{G}_{rel}\cdot ro\cdot ri\cdot\left(\left[Ca^{2+}\right]_{JSR} - \left[Ca^{2+}\right]_{ss}\right)$$

K. SR fluxes

Formulations for I_{up}, I_{leak}, and I_{tr} come from the LRd model[25]. The transfer rate of Ca^{2+} from the NSR to the JSR, τ_{tr}, is decreased from 180 ms to 120 ms to get faster refilling of releasable Ca^{2+} and less emptying of SR as reported experimentally[36]. Toyofuku et al. have identified Ser[38] as the site on SERCA2a phosphorylated by CaMKII[41]. They and others report increased $\overline{I}_{up}$ in response to CaMKII phosphorylation of SERCA2a[41,42], a finding which has been disputed[43,44]. Odermatt et al. argue that incubation of control cells in the presence of EGTA destabilizes the cells, producing an apparent CaMKII-dependent changes in $\overline{I}_{up}$ [43]. However, since then, Xu et al. have confirmed that CaMKII phosphorylation enhances $\overline{I}_{up}$ *in vitro*[45] and have reported phosphorylation of SERCA2a at Ser[38] *in vivo*[46], while a different group has measured decreased $\overline{I}_{up}$ in transgenic mice expressing a CaMKII inhibitory peptide[47]. Therefore, while controversy remains, mounting experimental evidence (*in vitro* and *in vivo*) supports the earlier findings that CaMKII phosphorylates SERCA2a to increase $\overline{I}_{up}$ [41,42]. Consistent with these data, the dependence of $\overline{I}_{up}$ on CaMKII is adjusted to produce a maximal increase of 75% (70% measured experimentally[41]), while the maximal CaMKII-dependent decrease in $K_{0.5}$ is 0.17 μmol/L[43] (to simulate effect of CaMKII on PLB, Online Data Supplement Figure 1).

$$\overline{\Delta}K_{m,PLB} = 0.00017 \text{ mmol/L};\ \overline{\Delta}I_{up,CaMK} = 0.75;\ K_{m,CaMK} = 0.15$$

$$\Delta K_{m,PLB} = \overline{\Delta}K_{m,PLB}\cdot\frac{CaMK_{active}}{K_{m,CaMK} + CaMK_{active}}$$

$$\Delta I_{up,CaMK} = \overline{\Delta}I_{up,CaMK}\cdot\frac{CaMK_{active}}{K_{m,CaMK} + CaMK_{active}}$$

$$I_{up} = \left(\Delta I_{up,CaMK} + 1\right)\cdot\overline{I}_{up}\cdot\frac{\left[Ca^{2+}\right]_i}{\left[Ca^{2+}\right]_i + K_{m,up} - \Delta K_{m,PLB}}$$

$\overline{I}_{up} = 0.004375$ mmol/L per ms; $K_{m,up}$ = 0.00092 mmol/L

$$\overline{NSR} = 15 \text{ mmol/L}$$

$$I_{leak} = \frac{0.004375}{\overline{NSR}} \cdot [Ca^{2+}]_{NSR}$$

$$\tau_{tr} = 120 \text{ ms}$$

$$I_{tr} = \frac{[Ca^{2+}]_{NSR} - [Ca^{2+}]_{JSR}}{\tau_{tr}}$$

L. Time-independent currents

Formulations for the time-independent currents with the exception of the Ca^{2+} background current, $I_{Ca,b}$, come from the LRd model[25]. Conductances are reduced to account for the smaller conductances of the major time-dependent currents in the HRd model.

a. $I_{Ca,b}$

$$I_{Ca,b} = P_{Ca,b} \cdot z_{Ca}^2 \cdot \frac{V_m \cdot F^2}{RT} \cdot \frac{\gamma_{Cai} \cdot [Ca]_i \cdot \exp\left(z_{Ca} \cdot V_m \cdot F / (RT)\right) - \gamma_{Cao} \cdot [Ca]_o}{\exp\left(z_{Ca} \cdot V_m \cdot F / (RT)\right) - 1}$$

$$P_{Ca,b} = 1.995084 \times 10^{-7} \text{ cm/s, ; } \gamma_{Cai} = 1; \gamma_{Cao} = 0.341$$

b. I_{NaK}

$$\sigma = \frac{\exp\left([Na^+]_o / 67.3\right) - 1.0}{7.0}$$

$$f_{NaK} = \frac{1}{1 + 0.1245 \cdot \exp\left(\frac{-0.1 \cdot V_m F}{RT}\right) + 0.0365 \cdot \sigma \cdot \exp\left(\frac{-V_m F}{RT}\right)}$$

$$K_{m,Nai} = 10 \text{ mM ; } K_{m,Ko} = 1.5 \text{ mM}$$

$$\overline{G}_{NaK} = 0.61875 \text{ mS/}\mu\text{F}$$

$$I_{NaK} = \overline{G}_{NaK} \cdot \frac{f_{NaK}}{1 + \left(\frac{K_{m,Nai}}{[Na^+]_i}\right)^2} \cdot \left(\frac{[K^+]_o}{[K^+]_o + K_{m,Ko}}\right)$$

c. I_{Kp}

$$E_{Kp} = \frac{RT}{F} \cdot \ln\left(\frac{[K^+]_o}{[K^+]_i}\right)$$

$$K_p = \frac{1}{1 + \exp\left(\frac{7.488 - V_m}{5.98}\right)}$$

$$\overline{G}_{Kp} = 2.76 \times 10^{-3} \text{ mS/}\mu\text{F}$$

$$I_{Kp} = \overline{G}_{Kp} \cdot K_p \cdot \left(V_m - E_{Kp}\right)$$

d. I_{K1}

$$E_{K1} = \frac{RT}{F} \cdot \ln\left(\frac{[K^+]_o}{[K^+]_i}\right)$$

$$\alpha_{K1} = \frac{1.02}{1 + \exp\left(0.2385 \cdot \left(V_m - E_{K1} - 59.215\right)\right)}$$

$$\beta_{K1} = \frac{0.49124 \cdot \exp\left(0.08032 \cdot \left(V_m - E_{K1} + 5.476\right)\right) + \exp\left(0.06175 \cdot \left(V_m - E_{K1} - 594.31\right)\right)}{1 + \exp\left(-0.5143 \cdot \left(V_m - E_{K1} + 4.753\right)\right)}$$

$$K_1 = \frac{\alpha_{K1}}{\alpha_{K1} + \beta_{K1}}$$

$$\overline{G}_{K1} = 0.5 \cdot \sqrt{\frac{[K^+]_o}{5.4}}\ \text{mS/μF}$$

$$I_{K1} = \overline{G}_{K1} \cdot K_1 \cdot \left(V_m - E_{K1}\right)$$

e. $I_{p,Ca}$

$$\overline{G}_{p,Ca} = 0.0575\ \text{mS/μF};\ K_{m,pCa} = 0.0005\ \text{mM}$$

$$I_{p,Ca} = \overline{G}_{p,Ca} \cdot \frac{[Ca^{2+}]_i}{K_{m,pCa} + [Ca^{2+}]_i}$$

M. Ca^{2+} buffers in myoplasm

$$\text{Buffered } [trpn] = [\overline{trpn}] \cdot \frac{[Ca^{2+}]_i}{[Ca^{2+}]_i + K_{m,trpn}}$$

$$\text{Buffered } [cmdn] = [\overline{cmdn}] \cdot \frac{[Ca^{2+}]_i}{[Ca^{2+}]_i + K_{m,cmdn}}$$

$[\overline{trpn}] = 0.07$ mmol/L; $[\overline{cmdn}] = 0.05$ mmol/L;
$K_{m,trpn} = 0.0005$ mmol/L ; $K_{m,cmdn} = 0.00238$ mmol/L

N. Ca^{2+} buffer in JSR

$$\text{Buffered } [csqn] = [\overline{csqn}] \cdot \frac{[Ca^{2+}]_{JSR}}{[Ca^{2+}]_{JSR} + K_{m,csqn}}$$

$[\overline{csqn}] = 10.0$ mmol/L; $K_{m,csqn} = 0.8$ mmol/L

O. Intracellular ion concentrations

a. Ca^{2+}

$$\frac{d[Ca^{2+}]_i}{dt} = -\left(\left(I_{Ca,b} + I_{p,Ca} - 2 \cdot I_{Na,Ca}\right) \cdot \frac{A_{Cap}}{V_{myo} \cdot 2F} + \left(I_{up} - I_{leak}\right) \cdot \frac{V_{NSR}}{V_{myo}} - I_{Diff} \cdot \frac{V_{ss}}{V_{myo}} \right)$$

$$[Ca^{2+}]_{i,t} = [trpn] + [cmdn] + [Ca^{2+}]_i + \Delta[Ca^{2+}]_i$$

$$b = [\overline{cmdn}] + [\overline{trpn}] - [Ca^{2+}]_{i,t} + K_{m,trpn} + K_{m,cmdn}$$

$$c = K_{m,cmdn} \cdot K_{m,trpn} - [Ca^{2+}]_{i,t} \cdot \left(K_{m,trpn} + K_{m,cmdn}\right) + [\overline{trpn}] \cdot K_{m,cmdn} + [\overline{cmdn}] \cdot K_{m,trpn}$$

$$d = -K_{m,trpn} \cdot K_{m,cmdn} \cdot [Ca^{2+}]_{i,t}$$

$$[Ca^{2+}]_i = \frac{2}{3}\sqrt{b^2 - 3c} \cos\left(\frac{1}{3} \cdot \cos^{-1}\left(\frac{9bc - 2b^3 - 27d}{2(b^2 - 3c)^{1.5}} \right) \right) - \frac{b}{3}$$

b. Na^+

$$\frac{d[Na^+]_i}{dt} = -I_{Na,t} \cdot \frac{A_{Cap}}{V_{myo} \cdot F} + CT_{NaCl}$$

c. K^+

$$\frac{d[K^+]_i}{dt} = -I_{K,t} \cdot \frac{A_{Cap}}{V_{myo} \cdot F} + CT_{KCl}$$

d. Cl-

$$\frac{d[Cl^-]_i}{dt} = I_{Cl,t} \cdot \frac{A_{Cap}}{V_{myo} \cdot F} + CT_{NaCl} + CT_{KCl}$$

P. SR calcium concentrations

a. JSR

$$\frac{d[Ca^{2+}]_{JSR}}{dt} = I_{tr} - I_{rel}$$

$$b = [\overline{csqn}] - [csqn] - [Ca^{2+}]_{JSR} - \Delta[Ca^{2+}]_{JSR} + K_{m,csqn}$$

$$c = K_{m,csqn} \cdot \left([csqn] + [Ca^{2+}]_{JSR} + \Delta[Ca^{2+}]_{JSR} \right);$$

$$[Ca^{2+}]_{JSR} = \frac{\sqrt{b^2 + 4c} - b}{2}$$

b. NSR

$$\frac{d[Ca^{2+}]_{NSR}}{dt} = I_{up} - I_{leak} - I_{tr} \cdot \frac{V_{JSR}}{V_{NSR}}$$

Q. Subspace calcium concentration

$$\beta_{ss} = \frac{1}{1 + \frac{\overline{BSR} \cdot K_{m,BSR}}{\left(K_{m,BSR} + [Ca^{2+}]_{ss}\right)^2} + \frac{\overline{BSL} \cdot K_{m,BSL}}{\left(K_{m,BSL} + [Ca^{2+}]_{ss}\right)^2}}$$

$\overline{BSR} = 0.047\,\text{mM};\ K_{m,BSR} = 0.00087\,\text{mM}$

$\overline{BSL} = 1.124\,\text{mM};\ K_{m,BSL} = 0.0087\,\text{mM}$

$$I_{Diff} = \frac{[Ca^{2+}]_{ss} - [Ca^{2+}]_i}{\tau_{Diff}}$$

$\tau_{Diff} = 0.2\,\text{ms}$

$$\frac{d[Ca^{2+}]_{ss}}{dt} = \beta_{ss}\left(-I_{Ca} \cdot \frac{A_{Cap}}{V_{ss} \cdot 2F} + I_{rel} \cdot \frac{V_{JSR}}{V_{ss}} - I_{Diff}\right)$$

R. Conservative current stimulus

A conservative current stimulus[48] with a duration of 1.0 ms and amplitude of -80 μA/μF is implemented during pacing protocols.

For duration of current stimulus,

$$I_{K,t} = I_{K,t} + 0.5 \cdot I_{stim}$$
$$I_{Cl,t} = I_{Cl,t} + 0.5 \cdot I_{stim}$$

S. V_m

$$\frac{dV_m}{dt} = \frac{-I_{tot}}{C_m}$$

T. Cell geometry

Length (L) = 0.01 cm; radius (r) = 0.0011 cm

Cell volume: $V_{cell} = \pi \cdot r^2 \cdot L = 38 \times 10^{-6}$ μL

Geometric membrane area: $A_{geo} = 2\pi \cdot r^2 + 2\pi \cdot r \cdot L = 0.767 \times 10^{-4}$ cm^2

Capacitive membrane area: $A_{cap} = R_{CG} \cdot A_{geo} = 1.534 \times 10^{-4}$ cm^2

Myoplasm volume: $V_{myo} = V_{cell} \cdot 68\% = 25.84 \times 10^{-6}$ μL

Mitochondria volume: $V_{mito} = V_{cell} \cdot 26\% = 9.88 \times 10^{-6}$ μL

SR volume: $V_{SR} = V_{cell} \cdot 6\% = 2.28 \times 10^{-6}$ μL

NSR volume: $V_{NSR} = V_{cell} \cdot 5.52\% = 2.098 \times 10^{-6}$ μL

JSR volume: $V_{JSR} = V_{cell} \cdot 0.48\% = 0.182 \times 10^{-6}$ μL

Subspace volume: $V_{ss} = V_{cell} \cdot 2.0\% = 0.76 \times 10^{-6}$

U. Miscellaneous comments

The T-type Ca^{2+} current, $I_{Ca(T)}$ is found in endocardial but not epicardial cardiac ventricular myocytes[49]. Therefore, the HRd model does not include $I_{Ca(T)}$.

In the LRd and HRd models, I_{NaCa} removes Na^+ from the cell at rest. In the LRd model, the background Na^+ current $I_{Na,b}$ allows for Na^+ entry to maintain homeostasis of $[Na^+]_i$ at rest. $I_{Na,b}$ is not included in the HRd model due to the presence of CT_{NaCl}, which brings Na^+ into the cell at rest.

$I_{Ca,K}$ and $I_{Ca,Na}$ are assumed to be insignificant and are eliminated from the HRd model.

REFERENCES

1. Schulman H. The multifunctional Ca^{2+}/calmodulin-dependent protein kinase. *Adv Second Messenger Phosphoprotein Res*. 1988;22:39-112.

2. Zhabotinsky AM. Bistability in the Ca^{2+}/calmodulin-dependent protein kinase-phosphatase system. *Biophys J*. 2000;79:2211-21.

3. Edman CF, Schulman H. Identification and characterization of δ_B-CaM kinase and δ_C-CaM kinase from rat heart, two new multifunctional Ca^{2+}/calmodulin-dependent protein kinase isoforms. *Biochim Biophys Acta*. 1994;1221:89-101.

4. Hagemann D, Kuschel M, Kuramochi T, Zhu W, Cheng H, Xiao RP. Frequency-encoding Thr^{17} phospholamban phosphorylation is independent of Ser^{16} phosphorylation in cardiac myocytes. *J Biol Chem*. 2000;275:22532-6.

5. Rubart M, Lopshire JC, Fineberg NS, Zipes DP. Changes in left ventricular repolarization and ion channel currents following a transient rate increase superimposed on bradycardia in anesthetized dogs. *J Cardiovasc Electrophysiol*. 2000;11:652-64.

6. Miyoshi S, Mitamura H, Fujikura K, Fukuda Y, Tanimoto K, Hagiwara Y, Ita M, Ogawa S. A mathematical model of phase 2 reentry; role of L-type Ca current. *Am J Physiol Heart Circ Physiol*. 2003;284:H1285-H1294.

7. Dolphin AC. Facilitation of Ca^{2+} current in excitable cells. *Trends Neurosci*. 1996;19:35-43.

8. Sculptoreanu A, Rotman E, Takahashi M, Scheuer T, Catterall WA. Voltage-dependent potentiation of the activity of cardiac L-type calcium channel $\alpha 1$ subunits due to phosphorylation by cAMP-dependent protein kinase. *Proc Natl Acad Sci USA*. 1993;90:10135-9.

9. Kamp TJ, Hu H, Marban E. Voltage-dependent facilitation of cardiac L-type Ca channels expressed in HEK-293 cells requires β-subunit. *Am J Physiol Heart Circ Physiol*. 2000;278:H126-36.

10. Greenstein JL, Wu R, Po S, Tomaselli GF, Winslow RL. Role of the calcium-independent transient outward current I_{to1} in shaping action potential morphology and duration. *Circ Res*. 2000;87:1026-33.

11. Cabo C, Boyden P. Electrical remodeling of the epicardial border zone in the canine infarcted heart: a computational analysis. *Am J Physiol Heart Circ Physiol*. 2003;284:H372-H384.

12. Zygmunt AC, Robitelle DC, Eddlestone GT. I_{to1} dictates behavior of $I_{Cl(Ca)}$ during early repolarization of canine ventricle. *Am J Physiol Heart Circ Physiol*. 1997;273:H1096-H1106.

13. Banyasz T, Fulop L, Magyar J, Szentandrassy N, Varro A, Nanasi PP. Endocardial versus epicardial differences in L-type calcium current in canine ventricular myocytes studied by action potential voltage clamp. *Cardiovasc Res*. 2003;58:66-75.

14. Sun H, Leblanc N, Nattel S. Mechanisms of inactivation of L-type calcium channels in human atrial myocytes. *Am J Physiol Heart Circ Physiol*. 1997;272:H1625-35.

15. Hirano Y, Hiraoka M. Ca^{2+} entry-dependent inactivation of L-type Ca current: a novel formulation for cardiac action potential models. *Biophys J*. 2003;84:696-708.

16. Li L, Satoh H, Ginsburg KS, Bers DM. The effect of Ca^{2+}-calmodulin-dependent protein kinase II on cardiac excitation-contraction coupling in ferret ventricular myocytes. *J Physiol (Lond)*. 1997;501:17-31.

17. Zuhlke R, Pitt G, Deisseroth K, Tsien R, Reuter H. Calmodulin supports both inactivation and facilitation of L-type calcium channels. *Nature*. 1999;399:159-62.

18. Fedida D, Noble D, Spindler AJ. Use-dependent reduction and facilitation of Ca^{2+} current in guinea-pig myocytes. *J Physiol (Lond)*. 1988;405:439-60.

19. Dzhura I, Wu Y, Colbran RJ, Balser JR, Anderson ME. Calmodulin kinase determines calcium-dependent facilitation of L-type calcium channels. *Nat Cell Biol*. 2000;2:173-7.

20. Liu DW, Antzelevitch C. Characteristics of the delayed rectifier current (I_{Kr} and I_{Ks}) in canine ventricular epicardial, midmyocardial, and endocardial myocytes. A weaker I_{Ks} contributes to the longer action potential of the M cell. *Circ Res*. 1995;76:351-65.

21. Lue WM, Boyden PA. Abnormal electrical properties of myocytes from chronically infarcted canine heart. Alterations in V_{max} and the transient outward current. *Circulation*. 1992;85:1175-88.

22. Liu DW, Gintant GA, Antzelevitch C. Ionic bases for electrophysiological distinctions among epicardial, midmyocardial, and endocardial myocytes from the free wall of the canine left ventricle. *Circ Res*. 1993;72:671-87.

23. Weber CR, Ginsburg KS, Philipson KD, Shannon TR, Bers DM. Allosteric regulation of Na/Ca exchange current by cytosolic Ca in intact cardiac myocytes. *J Gen Physiol*. 2001;117:119-31.

24. Weber CR, Piacentino V, Ginsburg KS, Houser S, Bers DM. Na^{+}-Ca^{2+} exchange current and submembrane $[Ca^{2+}]_i$ during the cardiac action potential. *Circ Res*. 2002;90:182-189.

25. Luo CH, Rudy Y. A dynamic model of the cardiac ventricular action potential. I. Simulations of ionic currents and concentration changes. *Circ Res*. 1994;74:1071-96.

26. Maltsev VA, Sabbah HN, Undrovinas AI. Late sodium current is a novel target for amiodarone: studies in failing human myocardium. *J Mol Cell Cardiol*. 2001;33:923-32.

27. Zygmunt AC, Eddlestone GT, Thomas GP, Nesterenko VV, Antzelevitch C. Larger late sodium conductance in M cells contributes to electrical heterogeneity in canine ventricle. *Am J Physiol Heart Circ Physiol*. 2001;281:H689-97.

28. Baumgarten CM, Duncan SWN. Regulation of Cl^- activity in ventricular muscle: Cl^-/HCO_3^- exchange and Na^+-dependent Cl^- cotransport. In: Dhalla NS, Pierce GN, Beamish RE, eds. *Heart Function and Metabolism*. Winnipeg, Cananda: Martinus Nijhoff; 1986:116-131.

29. Kneller J, Ramirez RJ, Chartier D, Courtemanche M, Nattel S. Time-dependent transients in an ionically based mathematical model of the canine atrial action potential. *Am J Physiol Heart Circ Physiol*. 2002;282:H1437-H1451.

30. Piwnica-Worms D, Jacob R, Horres CR, Lieberman M. Potassium-chloride cotransport in cultured chick heart cells. *Am J Physiol Cell Physiol*. 1985;249:C337-44.

31. Collier ML, Levesque PC, Kenyon JL, Hume JR. Unitary Cl^- channels activated by cytoplasmic Ca^{2+} in canine ventricular myocytes. *Circ Res*. 1996;78:936-44.

32. Sham J, Song L, Chen Y, Deng L, Stern M, Lakatta E, Cheng H. Termination of Ca^{2+} release by a local inactivation of ryanodine receptors in cardiac myocytes. *Proc Natl Acad Sci USA*. 1998;95:15096-101.

33. Fabiato A. Time and calcium dependence of activation and inactivation of calcium-induced release of calcium from the sarcoplasmic reticulum of a skinned canine cardiac Purkinje cell. *J Gen Physiol*. 1985;85:247-89.

34. Lukyanenko V, Gyorke I, Gyorke S. Regulation of calcium release by calcium inside the sarcoplasmic reticulum in ventricular myocytes. *Pflugers Arch*. 1996;432:1047-54.

35. DelPrincipe F, Egger M, Niggli E. Calcium signalling in cardiac muscle: refractoriness revealed by coherent activation. *Nat Cell Biol*. 1999;1:323-9.

36. Shannon TR, Guo T, Bers DM. Ca^{2+} scraps: local depletions of free $[Ca^{2+}]$ in cardiac sarcoplasmic reticulum during contractions leave substantial Ca^{2+} reserve. *Circ Res*. 2003;93:40-45.

37. Witcher DR, Kovacs RJ, Schulman H, Cefali DC, Jones LR. Unique phosphorylation site on the cardiac ryanodine receptor regulates calcium channel activity. *J Biol Chem*. 1991;266:11144-52.

38. Lokuta AJ, Rogers TB, Lederer WJ, Valdivia HH. Modulation of cardiac ryanodine receptors of swine and rabbit by a phosphorylation-dephosphorylation mechanism. *J Physiol (Lond)*. 1995;487:609-22.

39. Wu Y, Colbran RJ, Anderson ME. Calmodulin kinase is a molecular switch for cardiac excitation-contraction coupling. *Proc Natl Acad Sci USA*. 2001;98:2877-81.

40. Netticadan T, Xu A, Narayanan N. Divergent effects of ruthenium red and ryanodine on Ca^{2+}/calmodulin-dependent phosphorylation of the Ca^{2+} release channel (ryanodine receptor) in cardiac sarcoplasmic reticulum. *Arch Biochem Biophys*. 1996;333:368-76.

41. Toyofuku T, Curotto Kurzydlowski K, Narayanan N, MacLennan DH. Identification of Ser^{38} as the site in cardiac sarcoplasmic reticulum Ca^{2+}-ATPase that is phosphorylated by Ca^{2+}/calmodulin-dependent protein kinase. *J Biol Chem*. 1994;269:26492-6.

42. Hawkins C, Xu A, Narayanan N. Sarcoplasmic reticulum calcium pump in cardiac and slow twitch skeletal muscle but not fast twitch skeletal muscle undergoes phosphorylation by endogenous and exogenous Ca^{2+}/calmodulin-dependent protein kinase. Characterization of optimal conditions for calcium pump phosphorylation. *J Biol Chem*. 1994;269:31198-206.

43. Odermatt A, Kurzydlowski K, MacLennan DH. The v_{max} of the Ca^{2+}-ATPase of cardiac sarcoplasmic reticulum (SERCA2a) is not altered by Ca^{2+}/calmodulin-dependent phosphorylation or by interaction with phospholamban. *J Biol Chem*. 1996;271:14206-13.

44. Reddy LG, Jones LR, Pace RC, Stokes DL. Purified, reconstituted cardiac Ca^{2+}-ATPase is regulated by phospholamban but not by direct phosphorylation with Ca^{2+}/calmodulin-dependent protein kinase. *J Biol Chem*. 1996;271:14964-70.

45. Xu A, Narayanan N. Ca^{2+}/calmodulin-dependent phosphorylation of the Ca^{2+}-ATPase, uncoupled from phospholamban, stimulates Ca^{2+}-pumping in native cardiac sarcoplasmic reticulum. *Biochem Biophys Res Commun*. 1999;258:66-72.

46. Xu A, Netticadan T, Jones DL, Narayanan N. Serine phosphorylation of the sarcoplasmic reticulum Ca^{2+}-ATPase in the intact beating rabbit heart. *Biochem Biophys Res Commun*. 1999;264:241-6.

47. Ji Y, Li B, Reed TD, Lorenz JN, Kaetzel MA, Dedman JR. Targeted inhibition of Ca^{2+}/calmodulin-dependent protein kinase II in cardiac longitudinal sarcoplasmic reticulum results in decreased phospholamban phosphorylation at threonine 17. *J Biol Chem*. 2003;278:25063-71.

48. Hund TJ, Kucera JP, Otani NF, Rudy Y. Ionic charge conservation and long-term steady state in the Luo-Rudy dynamic model of the cardiac cell. *Biophys J*. 2001;81:3324-3331.

49. Wang H-S, Cohen IS. Calcium channel heterogeneity in canine left ventricular myocytes. *J Physiol (Lond)*. 2003;547:825-833.

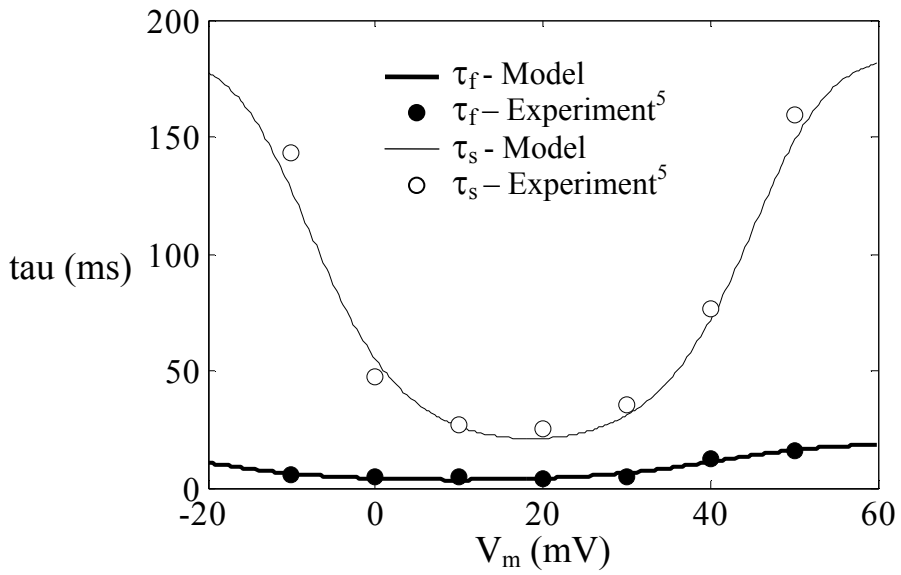

FIGURE E1 $I_{Ca(L)}$ fast (*thick line*) and slow (*thin line*) voltage-dependent inactivation time constants fitted to canine ventricular data[5] (*circles*).